Sterol transport protein ORP6 regulates astrocytic cholesterol metabolism and brain Aβ deposition

Viyashini Vijithakumar

Thesis submitted to the University of Ottawa
in partial Fulfillment of the requirements for the
Master of Science degree in Biochemistry

Department of Biochemistry, Immunology and Microbiology
Faculty of Medicine
University of Ottawa

ABSTRACT

The mammalian brain is the most cholesterol-rich organ of the body, requiring *in situ de novo* cholesterol synthesis to maintain its cholesterol requirement. Defects in brain cholesterol homeostasis are implicated in cognitive deficits related to aging and in neurodegenerative diseases such as Alzheimer's Disease (AD). Oxysterol-binding protein (OSBP) – related proteins are highly conserved cytosolic proteins that coordinate lipid homeostasis by regulating cell signaling, inter-organelle membrane contact sites and non-vesicular transport of cholesterol. Previously, ORP6, a poorly characterized member of this family, was found to be part of complex transcriptional cascade coordinated by SBREP2 and emerged as a novel regulator of intracellular cholesterol trafficking in hepatocytes and macrophages. Yet how ORP6 regulates these pathways and its function in the brain where it is most highly expressed is unknown. Here, we show that ORP6 is highly expressed in the brain, where it exhibits spatial and cell-type specific expression. ORP6 expression is enriched in the hippocampus and caudal-putamen brain regions, specifically within neurons and astrocytes. ORP6 knockdown in astrocytes altered the expression of cholesterol biosynthesis, cholesterol efflux and cholesterol esterification genes, resulting in the accumulation of esterified cholesterol within cytoplasmic lipid droplets and reduced cholesterol efflux highlighting a role for ORP6 in astrocytic cholesterol metabolism. We also present in this thesis, the newly generated second viable ORP family member knockout mouse. ORP6 ablation in mice results in the dysregulation of brain and whole-body lipid homeostasis, increased Aβ deposition in the brain and neuroanatomical alterations. Together, our findings highlight a critical role for cholesterol trafficking proteins in brain cholesterol homeostasis and identify ORP6 as a potential novel target for AD.

ACKNOWLEDGEMENTS

I would like to first and foremost convey my gratitude to Dr. Mireille Ouimet for believing in me and affording me the opportunity to broaden my knowledge of brain and cardiovascular metabolism under her supervision. Thank you for always providing me with multiple opportunities to grow and develop my skills to become a better scientist. The skills I have learned under your supervision will prove invaluable during my future career.

I would also like to thank all members of the Ouimet lab: Christina Emerton, Sabrina Robichaud, Arlette Kasongo, Dominique Boucher, Lara Gharibeh, Issraa Suliman, Thomas Laval, Garrett Fairman, Fereshteh Moradi and Valérie Rochon. It was a pleasure getting to know and work with each of you. I would like to specifically thank Christina Emerton for always being there to help and support me with any experiment and keeping the lab happy with her wonderful baking.

I would like to acknowledge my Thesis Advisory Committee members Dr. Diane Lagace and Dr. Baptiste Lacoste for their guidance with my project, your support, advice, and suggestions were invaluable.

I am very thankful for my parents, Viji and Bharathi and my brother, Vidulash for their continued support and encouragements throughout the course of my studies. I would like to also express my gratitude to my friends, particularly Renukha, Allison, Nabeeha, and Angelique for their constant moral support. Lastly, I would like to especially thank Pandu for the unconditioned support and patience during this journey. Thank you for always believing in me and for always encouraging me to stay positive even when times were hard.

TABLE OF CONTENTS

LIST OF ABBREVIATIONS

24-OHC	24-hydroxycholesterol
27-OHC	27-hydroxycholesterol
AB	Amyloid beta
ABC transporters:	ATP-binding cassette transporters
ABCA1	ATP binding cassette subfamily A member 1
ABCG1	ATP Binding Cassette Subfamily G Member 1
ABCG4	ATP Binding Cassette Subfamily G Member 4
ACAT1/SOAT1:	Acyl-coenzyme A: cholesterol acyltransferase
AD	Alzheimer's Disease
ApoA1	Apolipoprotein A-I
ApoD	Apolipoprotein D
ApoE	Apolipoprotein E
ApoF	Apolipoprotein F
ApoJ	Apolipoprotein J
Apol8	Apolipoprotein L 8
APP	Amyloid precursor protein
BBB	Blood Brain Barrier
CAA	Cerebral amyloid angiopathy
CAD	Coronary artery disease
CE	Cholesteryl ester
CNS	Central Nervous System
CVD	Cardiovascular Disease
CYP46A1	cholesterol 24-hydroxylase
CYP7A1	cytochrome P450 family 7 subfamily A member
CYP7B1	cytochrome P450 family 7 subfamily B member 1
DE	Desmosterol
DHCR24	24-Dehydrocholesterol reductase
DHCR7	7-Dehydrocholesterol reductase

ER	Endoplastic Reticulum
ESI	Electrospray ionisation
FA	Fatty acid
FFAT	Two phenylalanine in an acidic tract
HD	Huntington's Disease
HDL	High Density Lipoprotein
HMG-CoA:	3-Hydroxy-3-methylglutaryl CoA
HMGCS2	3-hydroxy-3-methylglutaryl-CoA synthase 2
HMGR	HMG-CoA reductase enzyme
IDOL	Inducible degrader of LDLR
IF	Immunofluorescence
KD	Knockdown
KO	Knockout
LD	Lipid Droplet
LDL	Low-density lipoprotein
LDLR	Low-density lipoprotein family receptor
LRP1	Lipoprotein receptor-related protein 1
LRP6	Lipoprotein receptor-related protein 6
LTP	Lipid Transfer Protein
LXR	Liver X receptor
LXRE	LXR Responsive Element
MCS	Membrane Contact Site
mβ-CD	Methyl-β-cyclodextrin
NPC1	Niemann Pick Type C protein 1
NPC2	Niemann Pick Type C protein 2
NSDHL	NAD(P) dependent steroid dehydrogenase-like
ORD	OSBP-related domain
ORP	Oxysterol Binding protein related protein
OSH	oxysterol-binding homology

P/S	Penicillin-streptomycin
PD	Parkinson's Disease
PFA	Paraformaldehyde
PH	Pleckstrin homology
PI4P	Phosphatidylinositol 4-phosphate
PM	Plasma Membrane
PNS	peripheral nervous system
PPI	Prepulse Inhibition
PS	phosphatidylserine
qRT-PCR	quantitative real-time PCR
RXR	Retinoid X receptor
SCAP	SREBP cleavage-activating protein
SREBP1	Sterol regulatory element-binding protein 1
SREBP2	Sterol regulatory element-binding protein 2
SSD	Sterol sensing domain
STARD1	Steroid acute regulatory protein
STARD3	StAR-related lipid transfer domain-3
TCP	The Centre for Phenogenomics
VAP	VAMP-associated protein
VLDL	Very-low-density lipoprotein cholesterol
WT	Wildtype

LIST OF FIGURES

LIST OF TABLES

1. INTRODUCTION

1.1 Cholesterol Homeostasis in the Brain

Cholesterol is an essential component of the human body and is vital for proper cellular and systemic function. It is synthesized by all cells and is predominantly found on cell membranes to modulate their rigidity, fluidity, and permeability[1]. Cholesterol is also a precursor for several other important components of the body including bile salts, steroid hormones and vitamin D[2].

The brain is the most cholesterol-rich organ of the body. While it takes up only 2.1% of the total body mass, it contains approximately 20% of the body's total cholesterol[3]. The majority of cholesterol in the brain (approximately 70%) is found in myelin sheaths formed by oligodendrocytes while the remaining 30% is metabolically active and found in the plasma membrane of astrocytes and neurons[4]. Within the brain, cholesterol is necessary for neuronal activity, neurotransmission, synaptogenesis, dendrite formation, and axonal guidance[4–7]. While it is evident that cholesterol is crucial for brain development and function, its dysregulation can lead to both structural and function central nervous system (CNS) diseases such as Alzheimer's disease (AD), Parkinson's disease (PD), Huntington's disease (HD) and Niemann-Pick C disease[8]. As such, the brain relies on precisely orchestrated processes to balance cholesterol synthesis, uptake, and excretion to continually maintain tight levels of cholesterol concentrations.

1.1.1 Cholesterol synthesis

Cholesterol biosynthesis begins in the ER with acetyl-CoA and involves over 30 enzymatic steps with the participation of at least 20 different enzymes[4]. The rate-limiting step in cholesterol biosynthesis is the conversion of 3-hydroxy-3-methylglytaryl-CoA (HMG-CoA) into mevalonate by the HMG-CoA reductase enzyme (HMGR)[9]. Mevalonate is eventually converted into lanosterol, upon which two different pathways have been suggested in the brain; the Bloch and the Kandutsch-Russel pathways[10]. In the Bloch pathway, desmosterol is converted to cholesterol by 24-dehydrocholesterol reductase (DHCR24), thus all intermediates following lanosterol up to

desmosterol will contain a Δ24 double bonds. In the Kandutsch-Russel pathway, DHCR24 acts directly on lanosterol itself, hence all following intermediates contain a saturated side chain[11]. In the brain, astrocytes preferentially utilize the Bloch pathway, while neurons tend to use the Kandutsch Russel pathway[6]. Recent studies have however also shown that developing neurons and astrocytes can both use the Bloch pathway to synthesize cholesterol[12], suggesting that as the neurons mature, they switch synthesis pathways.

Because the blood brain barrier (BBB) prevents the uptake of lipoproteins from the circulation, cholesterol homeostasis mechanisms in the brain differ from that of the peripheral nervous system, whereby CNS cholesterol requirements are entirely maintained by *in situ* de novo synthesis[9]. The rate of synthesis is highest during the perinatal phase, where oligodendrocytes synthesize cholesterol for myelin sheath that aids in rapid conduction of neuronal impulses[13]. Mounting evidence points to astrocytes as the predominant producers of cholesterol in the adult brain. As the brain matures, the requirement of cholesterol and its production are reduced[14,15]; yet, the expression of cholesterol biosynthesis enzymes and transcriptional control of cholesterol biosynthesis are the highest in astrocytes relative to other cell types of the CNS[16,17]. Moreover, studies have shown that glial-derived cholesterol is sourced by microglia for survival and phagocytosis, while neurons require it for synaptogenesis[5,18]. Ablation of cholesterol synthesis in astrocytes impacts social behavior, learning, memory, and motor coordination, further implicating glial cholesterol production in quantity and quality of neuronal synapses and overall brain function[7].

1.1.2 Cholesterol storage and excretion

When the intracellular levels of cholesterol exceed a cell's requirements, excess cholesterol can be removed through 3 pathways: 1) esterification and storage in cytoplasmic lipid droplets (LDs), 2) secretion via ABC transporters and 3) oxidized into oxysterols that cross the BBB and are excreted from the body[6,19].

Cholesterol esterification is catalyzed by ER-resident acyl-coenzyme A (CoA): cholesterol acyltransferase (ACAT/SOAT)[20]. The resulting cholesteryl ester (CE) is stored in cytoplasmic LDs. When cholesterol is subsequently needed, CE can be hydrolyzed by cytoplasmic neutral CE hydrolases[20] or lipophagy[21]. LD-associated CE accounts for only 1% of the total cholesterol in neurons[9], the remaining 99% of cholesterol being in the unesterified form[6]. While ACAT1/SOAT1 is more active in neurons than astrocytes, under conditions of excess cell cholesterol, its activity also increases in astrocytes[6].

Cells of the CNS express ABC transporter proteins such as ABCA1, ABCG1 and ABCG4 [6,9]. These transporters allow for cholesterol to be pumped out of the cell to cholesterol acceptors such as apoA1 and apoE[6,9]. Brain cholesterol is transported as a component of high-density lipoprotein (HDL)-like particles that are comparable to circulating peripheral HDLs in terms of their ability to bind, transport and deliver cholesterol[4]. The major apolipoprotein component of these particles is apoE that interacts with ABCA1 to form unesterified cholesterol-rich HDL-like particles[22]. These are subsequently secreted from astrocytes and taken up by neurons using LDLR transporters located on neuronal membranes[23,24]. Studies have observed different expression patterns of the ABC transporters on astrocytes and neurons. ABCA1 and ABCG1 primarily regulate glial cholesterol efflux while ABCG4 expression is more highly expressed in neurons allowing for neuronal cholesterol transportation[25]. This cell specificity expression pattern of ABC transporters suggests that cholesterol efflux is differentially regulated in distinct cell types of the CNS.

Lastly, the major excretory pathway for brain cholesterol is via hydroxylation of cholesterol by cholesterol 24-hydroxylase (encoded by CYP46A1) to generate 24-hydroxycholesterol (24-OHC). 24-hydroxylase is a neuron-specific enzyme, predominantly expressed in pyramidal cells of the cortex and Purkinje cells of the cerebellum[6]. There is very little expression of 24-hydroxylase in glial cells, indicating that the majority of cholesterol turnover takes place in neurons[6]. Newly formed 24-OHC is not only less toxic than cholesterol itself, but it can also readily cross the BBB due to its lipophilic nature by passive diffusion into the peripheral circulation to be excreted. Approximately 40-50% of brain cholesterol is removed through this pathway[6,9].

1.1.3 Transcriptional Regulation of Cholesterol in the brain

The tight regulation of cholesterol homeostasis is mediated by two main transcriptional axes; the SREBP transcription factors and nuclear receptors.

Master regulators of cholesterol synthesis in the ER are the sterol regulatory element-binding proteins (SREBPs)[11,26]. When cholesterol levels are low, activation of these transcription factors induce the expression of genes required for the biosynthesis of cholesterol. SREBPs are retained on the ER membrane through the association with SREBP cleavage activating protein (SCAP). In low cholesterol condition, the sterol sensing domain (SSD) of SCAP is no longer bound with cholesterol and initiates the release of SREBP to be transported to the Golgi [19,26]. Once in the Golgi, SREBP is cleaved by site 1 and 2 proteases that release its N-terminus into the cytoplasm, from where it is translocated to the nucleus and induces the expression of low-density lipoprotein receptor (LDLR), HMG-CoA reductase (HMGCR), Insig 1 to promote cholesterol synthesis and uptake[19,27]. Almost all genes that encode enzymes in cholesterol synthesis are targets of SREBPs[11]. SREBP also supresses the expression of ABCA1 to reduce cholesterol efflux and retain cellular cholesterol[27]. Conversely, when there is an increase in cellular cholesterol, the SREBP-SCAP complex remains anchored to the ER and the subsequent events do not take place. In the brain, studies have shown that depletion of SREBP2 from astrocytes results in impaired development and microencephaly along with behavioral and motor deficits[7]. Astrocyte-specific knockdown of SREBP2 also impacted neurite outgrowth suggesting a critical role for astrocyte cholesterol in brain development[7]. Additionally, mir-33, a microRNA co-transcribed with SREBP2 emerged as a critical regulator of cholesterol homeostasis. Namely, mir-33 acts with SREBPs to regulate intracellular cholesterol levels by post transcriptionally repressing genes involved in cholesterol efflux and HDL metabolism[28].

Liver X Receptors are transcription factors that belong to the nuclear receptor superfamily and are regulators of cholesterol homeostasis. These lipid-activated transcription factors are abundantly expressed in the liver and brain and form heterodimers with Retinoid X receptors (RXRs) and bind to LXR Responsive Element (LXRE)[23]. In the unbound state, RXR/LRX

heterodimers repress gene transcription by recruiting corepressors, whereas the binding of ligands induces a conformational change allowing for the release the corepressors and the subsequent binding of co-activators that results in transcription of cholesterol efflux target genes. These genes include apoE, ABCA1 and ABCG1[14,29]. Activation of LXR also indirectly decreases cholesterol uptake into the cell by upregulating inducible degrader of LDLR (IDOL), a gene that degrades LDL receptor (LDLR)[4]. Oxysterol ligands from the CNS include 24(S)-hydroxycholesterol (24-OHC), 22(R)-hydroxycholesterol, 24(S),25-epoxycholesterol, and 27-hydroxycholesterol (27-OHC)[7,30]. 24S-OHC produced in neurons can bind to LXR target genes in glial cells, subsequently increasing flux of cholesterol from astrocytes to neurons[30,31]. Recently, desmosterol has also been idenfied as a major physiological ligand for LXRs[11].

1.2 Cholesterol Transport

To maintain cholesterol homeostasis, synthesized cholesterol must travel to its final functional destination to exert its physiological functions[32]. Unlike proteins, lipids do not contain intrinsic motifs or undergo chemical modifications that dictate their partitioning to target membranes. Yet, cell organelle membranes have unique and distinct lipid concentrations and profiles[32,33]. Moreover, as cholesterol is consistently trafficked from is site of synthesis (ER) to the plasma membrane (PM), cholesterol concentration is always highest in the PM and lowest in the ER[32].

Intracellular lipid trafficking is mediated by either vesicular or non-vesicular transport mechanisms. Vesicular transport involves the incorporation of cholesterol into the membrane of transport vesicles using metabolic energy[9,32,34]. Interestingly, lipid transport was observed even under conditions in which vesicular transport was blocked by ATP depletion, indicating that lipid transport between organelles through other pathways is possible[32,35]. This led to the discovery of non-vesicular intracellular transport mechanisms, which have now emerged as important and prevalent pathways of trafficking in the cell[32,35]. Non-Vesicular transport involves lipid transfer proteins (LTPs) that pack cholesterol in a hydrophobic pocket and consequently shuttle through aqueous membranes[9]. This pathway of trafficking is facilitated at membrane contact sites

(MCSs), which are defined as small cytosolic gaps (approximately 30 nm) between the membranes of the ER and any the membrane of other cellular organelle[36]. At these sites, proteins can tether the two organelles and mediate the transfer of lipids through the aqueous cytoplasm by binding to the LTPs[9,36–38]. Despite the importance of transport and distribution of cholesterol within cells for normal physiological function, many questions remain about cholesterol transfer mechanisms between cell compartments. For most LTPs, it remains unclear whether they act as lipid carriers or lipid sensors or even both[39].

While the first LTP was discovered 50 years ago, the bulk of our knowledge on LTPs has only begun to emerge in the past few years[40]. Currently, multiple LTPs families exhibit the capacity for mediating sterol transfer *in vitro*, such as StARs, CERTs and ORPs. Recent examples include, StAR-related lipid transfer domain-3 (STARD3) that localizes at the ER-endosome contact site to modulate cholesterol distribution by delivering cholesterol to endosomes[41]. Similarly, STARD1 moves cholesterol from the outer mitochondrial membrane to the inner membrane[42]. Assigning a physiological role for these LTPs still remain challenging. Only a handful of intracellular cholesterol-transfer proteins were attributed clear physiological functions *in vivo:* Niemann Pick Type C proteins 1 and 2 (NPC1, NPC2) that are required for lysosome cholesterol transport[43], steroid acute regulatory protein 1 (STARD1) that is required for cholesterol traffic to the inner mitochondrial membrane[42,44] and more recently Aster proteins that shuttle cholesterol between ER-PM contact sites[45]. Despite extensive study of these proteins, many questions remain about cholesterol transfer mechanism between cell compartments, namely within the brain.

1.3 Oxysterol binding protein-related proteins.

Oxysterol binding-related proteins (ORPs) constitute an enigmatic eukaryotic family of LTPs that facilitate non-vesicular transfer of cholesterol between lipid bilayers, increasing the efficiency of cholesterol transport between sub-cellular organelle membranes[46,47]. ORPs can also act as sterol regulators and sensors that relay information and activate signaling pathways[48].

There are currently 12 known ORPs in mammals, which are subdivided into six groups according to their amino acid sequence homology and domain organization (**Figure 1**). These 12 ORP genes give rise to 16 different protein variants through alternative splicing and transcription[49], each ORP possessing distinct sub-cellular localization patterns, functions, and tissue expression patterns[50]. Each OSBPL gene encoding for ORPs are found on different chromosomes, implying that they did not arise as a result of duplication of a single gene and, instead, they must have a different important function within the cell[38]. In *Saccharomyces cerevisiae*, deletion of all Osh proteins is lethal; however, expression of any one OSH gene prevents lethality, implying that all Osh homologs share at least one essential function in the cell[51]. Similarly, the collective deletion of all *Caenorhabditis elegans* homologs, OBR-1 to OBR-4, is embryonic lethal[52]. In turn, understanding the physiological role of ORPs in mice has proven difficult due to a lack of available genetic mouse models. An attempt at deleting OSBP in mice was unsuccessful as OSBP knockout mice die at an early embryonic stage, highlighting its critical importance for survival but leaving its essential physiologic function unknown[53]. Recently, the first viable ORP knockout mouse model was successfully developed, whereby systemic ORP8 deletion in mice resulted in elevated circulating HDL-cholesterol and sex- and diet-specific alterations in lipid metabolism[54]**.**

1.3.1 Functional Domains of ORPs

Our current structural and functional knowledge of ORPs has been extracted from extensive studies on the seven yeast *Saccharomyces cerevisiae* OSBP homologues (OSH) genes[39]. From these studies, two main structural components were identified in ORPs: the OSBP-related domain (ORD) and the pleckstrin homology (PH) domain (**Figure 1**). The C-terminal ORD is highly conserved between ORP members and binds sterols such as oxysterols and cholesterol. It contains the "OSBP fingerprint region" EQVSHHPP sequence motif fully conserved in all ORP members[38,39]. The PH domain is located on the N-terminus and interacts with phosphoinositides (PI4P) typically found in distinct non-ER organelle membranes. In addition to the PH domain, the N-terminus can also contain a two phenylalanine in an acidic tract (FFAT) motif and/or ankyrin repeats[39,47,55]. An FFAT motif is found on 8 of the mammalian ORPs and binds to VAMP-associated protein (VAP) found on the ER membrane, whereas the ankyrin repeats mediate interaction with

membrane-associated regulatory proteins. Replacing the FFAT motif, ORP5 and ORP8 contain a single C-terminal transmembrane domain that denotes their binding to the ER[50]. The FFAT motif and PH domain play a crucial role in targeting ORPs to specific ER and PIP-rich non-ER membrane compartments respectively, a property designated as 'dual membrane targeting'[49].

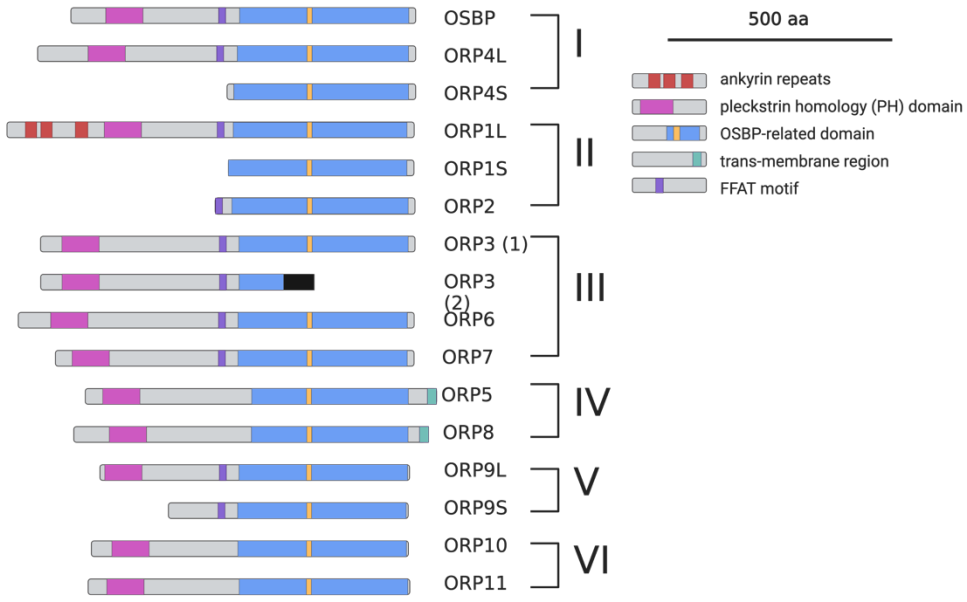

Figure 1. Structural domain organization of oxysterol-binding protein related proteins (ORPs). Schematic of ORP family protein domains in mammals. ORPs are divided into subgroups based on their sequence homology and domain organization, designated with Roman numerals. Created with Biorender.com.

1.3.2 Ligands of ORPs

OSBP, the founding member of the ORP family, was initially identified to bind to 25-OHC and thus was accordingly named oxysterol-binding protein[56]. However, upon cloning ORPs using OSBP and subsequent structural analysis and *in vitro* binding/transport assays, oxysterols, cholesterol and phospholipids were also identified as ligands for the members of the family. These ligands include: 24S-OHC, 22(R)-OHC, 7-ketocholesterol, PI4P and phosphatidylserine (PS) [39,55]. Several ORPs have demonstrated the ability to mediate the transfer of two ligands in opposite directions at MCSs. For example, OSBP functions in the exchange of cholesterol and PI4P at the Golgi complex-ER contact site[57]. Similarly, ORP5 and ORP8 mediate the counter transport of PI4P and PS at the ER-PM contact site[58]. The ability of ORPs to counter transport lipids has implication in lipid homeostasis regulation and trafficking.

1.4 A role for ORP6 in cholesterol homeostasis

Thus far, within the ORP family of 12 genes, six genes have been implicated in cholesterol transport: OSBP, ORP1L, ORP1S, ORP2, ORP5 and ORP6[59]. Of these, ORP6 remains the least studied. In a large genome-wide linkage scan for coronary artery disease (CAD), the ORP6 gene *OSBPL6,* was found to reside in a locus on chromosome 2 linked to premature CAD[60]. Subsequently, hepatic *OSBPL6* expression was positively correlated with plasma levels of high-density lipoprotein (HDL)-cholesterol, while reduced *OSBPL6* expression was observed in human carotid atherosclerotic plaques as compared to healthy arteries[61]. In macrophages, ORP6 was up-regulated in response to excess cholesterol and conversely down-regulated following cholesterol depletion[62]. Additionally, ORP6 was identified as part of a complex transcriptional cascade coordinated by SREBP2 and as an LXR-regulated gene and the most highly repressed target of miR-33[61]. ORP6 contributed to macrophage cholesterol homeostasis by regulating cholesterol trafficking between intracellular compartments and the plasma membrane for efflux[61]. While it appears to function in the homeostasis of cholesterol in macrophages, transcriptomic analysis reveal that ORP6 is most abundant in the brain, heart and skeletal muscle yet its role in the brain is poorly understood[38,63,55]. In both mouse and human brains, ORP6 expression is specifically enriched in astrocytes and neurons[64]. Studies in neurons have also identified ORP6 as a player in

the counter-transport of PI4P and PS by localizing to ER-PM contact sites[65,66]. However, ORP6's role in regulating glial cholesterol homeostasis remains unexplored. Interestingly, it was recently discovered that a single nucleotide polymorphism in the *OSBPL6* gene has genome-wide significance for association with Alzheimer's Disease[67]. Collectively, these data suggest an important physiological role for ORP6 in the CNS.

1.5 Cholesterol Homeostasis in Alzheimer's Disease

Alzheimer's Disease (AD) is a neurodegenerative disease clinically characterized by the progressive impairment of behavioral and cognitive functions[68]. Both genetic and environment factors can contribute to the development of the disease[69]. Association studies have identified candidate genes that increase the risk of developing AD. Interestingly, the dysregulation of several genes involved in cholesterol homeostatic pathways have been implicated in AD pathology, providing a link between cholesterol homeostasis and AD progression[70]. Most notably, one of the major genetic risk factors of AD is the presence of the ε4 allele of the ApoE gene, the main lipoprotein component binding to and shuttling cholesterol in the brain[71]. Inheriting the ApoE ε4 allele results in accelerated Amyloid Beta (Aβ) production. By binding to Aβ, ApoE can modify its aggregation and clearance rate, thus impacting the formation of amyloid plaques[72]. In contrast, the ApoE ε4 isoform has increased binding abilities to Aβ, thus preventing its binding to LRP1 for clearance[72]. Proper lipidation of HDL particles is crucial to maintain HDL function and the transportation of cholesterol to neurons. Lipidation degrees are also isoform-dependent, with ApoE ε4 isoform being the most poorly lipidated thus forming small HDL-like particles and reducing cholesterol transport to neurons[72]. Polymorphisms in other cholesterol homeostasis pathway genes include ApoJ, LRP, CYP46A1, ABCA1 and ACAT1 that are associated with AD risk, further establishing a clear link between cholesterol homeostasis and AD[73].

Although peripheral and CNS cholesterol metabolism are independent, the crossover of lipid species remains underestimated[74]. Several epidemiological studies have shown an inverse relationship between HDL and AD risk, whereby increased circulating HDL is associated with decreased risk of AD and vice versa[72,75–77]. A number of loci for proteins found on HDL such as

ApoE, ApoJ, SORL1 have been found to have genome-wide associations with AD risk[78]. Moreover, recent evidence supports a protective role for HDL against memory deficits, neuroinflammation and cerebral amyloid angiopathy (CAA), whereby HDL reduces vascular Aβ accumulation and reduces Aβ-induced endothelial inflammation[79].

Two neuropathological hallmarks of AD are 1. the accumulation of extracellular amyloid plaques composed of β-amyloid peptides and 2. The formation of intracellular neurofibrillary tangles composed of hyperphosphorylated tau[69]. Amyloid precursor protein (APP) can be cleaved by α-, β- or γ-secretases enzymes. The majority of APP is cleaved by α-secretase, producing αAPP and preventing the generation of Aβ (non-amyloidogenic pathway). Aβ is produced when APP is sequentially cleaved by β and γ-secretase instead (amyloidogenic pathway)[80]. Emerging evidence links alterations in intracellular cholesterol synthesis and efflux in the production of Aβ[81]. For example, increased ACAT1/SOAT1 activity in neurons indirectly promotes Aβ accumulation by reducing 24-OHC levels[82]. Conversely, ACAT1 deficiency could lead to an accumulation of cholesterol that is subsequently converted to 24S-OHC by Cyp46A1, reducing the available cholesterol[83]. Likewise, excess brain cholesterol by overexpression of SREBP2 also results in increased β-secretase and BACE1 activity and Aβ accumulation[84,85]. Furthermore, altered neuronal membrane cholesterol content results in aberrant formation, toxicity, and degradation of Aβ[86]. More specifically, when cholesterol transport to the PM is disrupted, abnormal Aβ metabolism and NFT are observed[87]. APP, β- and γ-secretases all localize to cholesterol-rich membrane domains[88–90]. In neurons, Aβ production has been attributed to the participation of lipid rafts in APP metabolism, and increased membrane cholesterol content shifts APP processing from non-amyloidogenic to amyloidogenic processing, resulting in increased Aβ production[91]. While cholesterol regulation in neurons has been extensively studied, less is known about the role of cholesterol regulation in astrocytes.

1.6 Research Plan

1.6.1 Rationale

ORP6 regulates macrophage and hepatocyte cholesterol efflux, yet its role in the brain, where it is most highly expressed, remains unknown. Limited studies have investigated ORP6, and fewer studies have investigated the role of ORP6 in brain cholesterol homeostasis. My thesis research project aimed to elucidate the role of ORP6 in cholesterol homeostasis the CNS, both *in vitro* and *in vivo*.

1.6.2 Objective

The objective of this thesis is to investigate the role of ORP6 in the CNS *in vitro* and *in vivo*.

1.6.3 Hypothesis

We hypothesized that ORP6 regulates cholesterol homeostasis in the central and peripheral nervous systems.

1.6.4 Aims

We tested our hypothesis with the following 3 aims:

1. Quantify ORP6 expression in the CNS.
2. Investigate the role of ORP6 in regulating cholesterol homeostasis in CNS cells, *in vitro*.
3. Investigate the role of ORP6 in whole body lipid homeostasis, *in vivo*.

2. MATERIALS AND METHODS

2.1 In Vitro

2.1.1 Cell culture

Mouse astrocyte-like cells C8-D1A, C8-S, C8-D30 (astrocyte type I, II and III clones), neuroblastoma-like cell (N2A) and microglia (BV2) cell lines were obtained from the American Type Culture Collection (ATCC). Cells were grown and maintained in Dubelcco's Modified Eagle Media (DMEM) (Corning, 10013CV) supplemented with 10% fetal bovine serum (FBS) and 1% penicillin-streptomycin (P/S) (Gibco, 15140122). All cells were maintained at 37ºC and 5% CO2 with medium replacement every 2-3 days. Cells were briefly washed with Hank's balanced salt solution (HBSS) (Gibco, LS14175103) then separated from culture dishes by trypsination (0.05% trypsin; Gibco 15400054)

2.1.2 siRNA transfection

For ORP6 gene silencing, C8-D1A cells were grown for 24h to 70% confluence and transfected with 25nM of *Osbpl6* SMARTpool On-TARGETplus siRNA (Dharmacon) using Lipofectamine RNAiMax Transfection Reagent (Invitrogen). Control samples were treated with an equal concentration of a non-targeting control sequence (ctrl siRNA) to control for non-specific effects in siRNA experiments. 24h post-transfection, an equal volume of 20% FBS culture media was added to the transfection mixture, RNA or protein were harvested 48h post-transfection.

2.1.3 Methyl-beta-cyclodextrin (mβ-CD)-cholesterol complexes

mß-CD cholesterol was prepared as previously described[92] by adding methyl-beta cyclodextrin (Sigma, C4555-10G) and cholesterol (Sigma, C8667-5G) with a mß-CD/cholesterol molar ratio of 8:1 in plain DMEM. An Ultrasonic Bath 2.8L (Fisher Scientific) was used to sonicate this mixture for 3 min at 37°C, and was incubated on a rotator overnight at 37°C, and complexes were filter-sterilized prior to use. 100µg/mL of mβ-CD-cholesterol was then used to load the cells.

2.1.4 Western blot

Cells treated with control or ORP6 siRNA were washed with PBS and scraped with RIPA lysis buffer (Tris-EDTA-EGTA, Complete protease inhibitor; Roche). Tissue samples were directly homogenized in RIPA lysis buffer. Samples were centrifuged every 5 mins for 30 mins on ice. Protein quantification was performed using Pierce 660nm Protein Assay Reagent (Thermofisher, 22660). Total protein samples (40-60 ug) in 4x Laemmli sample buffer (Bio-Rad, 1610747) were denatured by heating at 95°C for 10 mins and electrophoresed on 7.5% TGX Stain-Free™ FastCast™ Acrylamide gels (Bio-Rad, 1610181) with All Blue Precision marker (Bio-Rad, 1610393). Activated gels were transferred to 0.22 μm PVDF membranes for 10 min using the Trans-Blot Turbo Transfer System (Bio-Rad). Membranes were blocked in 5% milk in TBST for 1h, after which they were incubated with anti-ORP6 (1:500, Novus Biologicals NBP1-31456); anti-adipophilin (1:1000, Fitzgerald 20R-AP002); anti-ACAT1, 1:200, Santa Cruz, sc-20951), anti-APP (1:1000, Thermofisher PA5-17829), anti-DHCR24 (1:1000, Cell signaling 2033S), and anti-GAPDH (1:10000, Thermofisher, AM4300) at 4°C overnight. An enhanced HRP-based chemiluminescence detection system and HRP-conjugated secondary antibodies from Amersham Biosciences and Clarity, Clarity Max Chemiluminescence Reagent (Bio-Rad) or SuperSignal West Atto Ultimate Sensitivity Substrate (Thermofisher) were used to detect proteins with a ChemiDoc XRS+ System (Bio-Rad). For extracellular protein purification, the supernatant of cells treated as above with control or ORP6 siRNA was collected and centrifuged at 900Xg for 5 mins following the addition of a mixture of MeOH-$CHCl_3$-H_2O (4:1:3, v/v). Protein in the interface between the organic and the aqueous phases were precipitated with MeOH, spun at 900Xg for 10 mins, and pellets were re-suspended in RIPA lysis buffer for western blotting as above. Densitometric quantification and analysis were completed by Image Lab 6.1 Software (Bio-Rad).

2.1.5 RT-PCR analysis

Total RNA was isolated from cells using 400 μL of Trizol and Direct-Zol RNA MiniPrep Kit (Zymogen, R2052) according to the manufacturer's protocol. 350 ng of total RNA was reverse transcribed into complimentary DNA (cDNA) using the iScript Reverse Transcription Supermix for

qRT-PCR (Bio-Rad, 1708841) on the Mastercycler gradient (Eppendorf). Synthesized cDNA was diluted to the appropriate dilution based on primer optimization experiments. Expression was quantified by real-time PCR using BioRad Connect with SsoAdvanced SYBR Green Supermix (Bio-Rad). Expression data was normalized to SRP14 and GAPDH and expressed as fold change to control sample. Primer sequences are indicated in **Table 1**.

Table 1. Mouse qPCR primer sequences for gene expression analysis.

Gene	**Forward (5' – 3')**	**Reverse (5' – 3')**
Osbpl6	CTGGAGACCAGGTTCTCTGC	ATGTAGCGTCTTCGCGATCT
Plin2	GTGTGGTGATCTGGACCGTG	CTCATCACCACGCTCTGTTG
Soat1	GTGGAGCATTCGTTCAGGGAT	ATGTGACTGACGCTAGGATGA
Dhcr24	CTCTGGGTGCGAGTGAAGG	TTCCCGGACCTGTTTCTGGAT
Srp14	GAGAGCGAGCAGTTCCTGAC	CGGTGCTGATCTTCCTTTTC
Gapdh	AGGTCGGTGTGAACGGATTTG	TGTAGACCATGTAGTTGAGGTCA

2.1.6 PCR array gene expression profiling

Total RNA was extracted from C8-D1A cells treated with control siRNA, as described above. Reverse transcription was performed on 500ng total RNA using the RT2 First Strand kit (Qiagen, 330401) and quantitative real-time PCR (qRT-PCR) analysis of 84 key genes involved in lipoprotein signaling and cholesterol metabolism was performed using Mouse Lipoprotein Signaling & Cholesterol Metabolism RT^2 Profiler PCR Arrays (Qiagen, PAMM-080ZD) as per the manufacturer's protocol. Data analysis was performed using the manufacturer's integrated web-based software package for the PCR Array System using ΔΔCt based fold-change calculations.

2.1.7 Cholesterol efflux

For the quantification of exogenously delivered ^{3}H-cholesterol efflux, C8-D1A cells were transfected in 24-well plates with control or ORP6 siRNA complexed to RNAiMAX. Briefly, 100 µL of cells (1x10^5 cells / well) were added in OPTI-MEM to siRNA mixtures. 24h post-transfection, 100 µL of 20% FBS media containing 1 µCi/mL ^{3}H-cholesterol (Perkin Elmer, NET139001MC) and 100µg/mL mβ-CD-cholesterol was added. 24h post-lipid loading, media was replaced with

2mg/mL fatty acid-free BSA DMEM and cells were equilibrated for 2h. Media was then replaced with 50µg/mL of ApoA1, HDL or ApoE in 2mg/mL fatty acid free BSA DMEM for 4h, following which supernatants were removed and cells were lysed in 0.5M NaOH for 2 hours. 50µl aliquots of supernatants and cell lysates were transferred onto 96-well Lumaplates (Perkin Elmer, 6006633), dried overnight and radioactivity within samples was quantified using the Hydex Sense Plate reader (Gamble). Cholesterol efflux was calculated as a percentage of ^{3}H-cholesterol in the supernatant/(^{3}H-cholesterol in the supernatant + ^{3}H-cholesterol in cells)x 100%. For each experiment (n=4), fold-change efflux for each siRNA treatment was calculated relative to the average of control wells (scrambled ctrl siRNA). Human recombinant apoA-I was synthesized and purified as previously described[93], and confirmed endotoxin-free using the Chromogenic Endotoxin Quant Kit (Pierce, A39552). HDL was isolated from human plasma by sequential density ultracentrifugation as previously described[93] and apoE was purchased from Abcam (ab50242).

2.1.8 Lipid quantification by TLC

For total cholesterol ester quantification of exogenously delivered ^{3}H-cholesterol, BSA efflux samples from the cholesterol efflux experiments described above were neutralized with 2.5M HCl. Lipids were extracted from cell lysates using the Bligh and Dyer method[94]. For quantification of de *novo* synthesized cholesterol and intermediates in the Bloch cholesterol biosynthesis pathway, C8-D1A cells (5x10^{5} cells/well) cultured on a 6-well plate were transfected with control or ORP6 siRNA complexed to RNAiMAX in OPTI-MEM. 24h post-transfection, cells were labeled with 20µCi/mL ^{3}H-mevalonate for 24h (Perkin Elmer NET602) in 10% FBS DMEM media. Cells were cooled at 4°C for 15 mins and washed 2 times with ice-cold PBS and subsequently incubated with 10mM of mβ-CD at 4°C for 15 mins for cholesterol extraction from the plasma membrane. Intracellular lipids were extracted from cell lysates using the Bligh and Dyer method[94]. Lipid samples and standards were dissolved in hexane carrier and separated by thin layer chromatography on silica gel plates using a non-polar solvent system (hexane/diethyl ether/acetic acid, 70:30:1, v/v) for separation of cholesterol esters synthesized from exogenously delivered ^{3}H-cholesterol, or chloroform/acetone (99:1, v/v) for quantification of desmosterol. For

desmosterol resolution, TLC plates were run 3 times in the same solvent system and the plates were dried after each run. Lipid bands were visualized using iodine, scrapped, supplemented with 3 mL of EcoLite (+) Liquid Scintillation Cocktail (MP Biomedicals) and counted for radioactivity using Tri-Carb 4810 TR (PerkinElmer) for exogenous lipid samples.

2.1.9 Fluorescence microscopy

Cells were seeded on 8-well removable chamber slides (Ibidi) and fixed with 4% paraformaldehyde (PFA) (Alfa Aesar, 433689M) for 10 mins at room temperature following incubation with 100 µg/mL mβ-CD-cholesterol. For immunofluorescence (IF) of astrocytes, cells were washed 3X in 1X PBS and fixed in 4% PFA for 10 mins at 37°C. Cells were blocked/permeabilized for 30 min at room temperature in 5% BSA/0.01% Saponin. Cells were then incubated with anti-ORP6 (1:500, Novus NBP1-31456) overnight at 4°C in wash buffer containing 1% BSA/0.025% Saponin (Sigma, S7900). Alexa Fluor or Alexa Fluor Plus antibody conjugates (1:500-1:1000, Invitrogen) were incubated for 1 h at 37°C in wash buffer. Cells were incubated with BODIPY 493/503 (10 µg/mL, Invitrogen, D3922) for 30 mins at room temperature where indicated to stain neutral lipids and Fillipin (1:20, Sigma, F9765-25MG) for 20 mins where indicated to stain for free cholesterol. Cells were counterstained with DAPI (Invitrogen, D1306) for 5 mins at room temperature or DRAQ5 (1:1000, Biolegend 424101) for 10 mins. Slides were mounted on #1,5 coverslips (Ibidi, 10811) with DAKO mounting media (Agilent, S302380-2) and let dry overnight. Images were captured on a Zeiss LSM880 confocal microscope with a 63X objective (NA 1.4) using the appropriate lasers and the Airyscan module.

2.2 In Vivo

2.2.1 Mouse Tissue Collection

For ORP6 expression in mouse organs, 3 males and 3 females C57BL/J mice were sacrificed at 8 weeks. Brain, heart, liver, spleen, WAT, kidney and lungs were collected and split in half. For protein analysis, one half of each organ samples was homogenized in 1 mL of RIPA lysis buffer (89900, ThermoFisher) with a homogenizer for 5 mins (Polytron PT 1600E). Samples were rotated for 1hr at 4˚C then centrifuged at 20 000 rpm for 20 mins and the supernatants were collected for subsequent western blot. For mRNA expression quantification, samples were homogenized in 1 mL Trizol and then 200 uL of choroform (1/5 v:v) was added. Samples were inverted multiple times for 15 secs until a uniform pink suspension was obtained. Samples were then incubated at room temperature for 10 mins and then centrifuged at 12 000 xg for 15 mins at 4˚C. The upper aqueous phase was then transferred to a new tube and RNA was isolated using the Direct-Zol RNA MiniPrep Kit (Zymogen, R2052) according to the manufacturer's protocol.

2.2.2 Generation of Osbpl6-/- Mouse

All procedures involving animals at The Centre for Phenogenomics (TCP) were performed in compliance with the Animals for Research Act of Ontario and the Guidelines of the Canadian Council on Animal Care under protocols reviewed and approved by TCP Animal Care Committee. Animals were housed at a density of 2–5 animals per cage in individually ventilated cages (Tecniplast Sealsafe Plus). Envigo Teklad 2918X diet, quarter-inch corn cob bedding substrate and environmental enrichment of shredded paper (Enviropak) were provided. Room temperature was 21-22˚C and humidity was regulated at 30-55%.

The mouse line C57BL6/N-*Osbpl6*$^{em1(IMPC)Tcp}$/Cmmr was made as part of the International Mouse Phenotyping Consortium project[95] at The Centre for Phenogenomics using published protocols[96]. It was obtained from the Canadian Mouse Mutant Repository. Briefly, C57BL/6NCrl zygotes were electroporated with 8 µM of Cas9 protein (IDT) complexed with in house synthesized guide RNAs with spacers targeting introns flanking *Osbpl6* exon 10 (ENSMUSE00001282206) (Figure 2, **Table**

2). Treated zygotes were transferred to pseudopregnant CD-1 recipients for parturition and birth. Born pups were genotyped by end-point PCR (Table 3) and a founder with exon 10 deleted was selected for backcross to C57BL/6NCrl mice. N1 pups were identified using by PCR for the deletion allele (*Osbpl6*_wtF_F1 + *Osbpl6*_wt_R1 = 698 bp), the deletion amplicon sequenced to identify the allele sequence, and N1 mice with the exact same allele sequence used to establish the line. Heterozygous *Osbpl6*$^{+/-}$ mice were intercrossed in pairs to generate homozygous *Osbpl6*$^{-/-}$ to test viability and generate phenotyping cohorts. Born pups were biopsied at 13-17 days of age to identify wild-type, heterozygous, and homozygous mice and these data are reported in **Figure 6**.

Table 2. Sequences used to generate *Osbpl6*$^{-/-}$ mice.

Name	Sequence (5'-3')	Target site
Osbpl6_gRNA_E10U	TGATCATGGTTCCGCCCTCA	Chr2: 76385103-76385122 (-1)
Osbpl6_gRNA_E10D	ATTCTTCTAGGCGTAACAAT	Chr2: 76385709-76385728 (+1)

Table 3. Genotyping primer sequences for *Osbpl6*$^{-/-}$ mice.

Name	Sequence (5'-3')	Target site
Osbpl6_wt_FP1	TGCATGAAACCAGGCCTTAGATATA	Chr2: 76384790-76384814 (+1)
Osbpl6_wt_RP1	AATACCAAAGAGAACTGGGAGTTGA	Chr2: 76385913-76385937 (-1)
Osbpl6_wtF_FP2	AAAGGGAAGTTACTATTCACAGGCT	Chr2: 76385550-76385574 (+1)

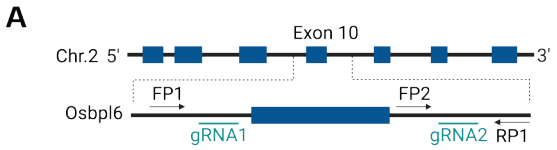

Figure 2. CRISPR/Cas9-mediated generation of *Osbpl6*$^{-/-}$ mice.

(A) CRISPR-Cas9 mediated 1000-bp deletion within exon 10 of *Osbpl6* on chromosome 2, utilizing a pair of guide RNAs (gRNA1, gRNA2).

2.2.3 Clinical phenotyping of Osbpl6-/- Mice

Comprehensive phenotyping of *Osbpl6*$^{-/-}$ mice was performed using the International Mouse Phenotyping Resource of Standardised Screens (IMPReSS). All data is available at the International Mouse Phenotyping Consortium web portal[97](mousephenotype.org). Detailed protocols can be found at the portal. Grip strength tests were performed at 9 weeks of age and are the average of 3 independent trials normalized to body weight. For these, the mouse was held at the base of the tail, lowered over the top of a grid so that only its front paws can grip the grid and pulled back steadily until the grip is released down the complete length of the grid. This procedure is repeated three times (trials) before three more trials are done allowing the use of both forelimbs and hind limbs together (EB1-BIO-GT3 Grip Strength Meter, EB Instruments). PPI startle tests were performed at 10 weeks of age. During all testing, the background was set at 65-dB white noise. Prepulse intensity was set at background, 70, 75, 80, 85 dB, and the startle stimulus in each case was 110 dB. These data are reported in **Figure 4**.

2.2.4 Lipidomics analyses

Lipidomics analyses were performed at the Montreal Heart Institute Metabolomic platform using a previously described and validated workflow[98,99]. In brief, frozen plasma or snap frozen brains samples of 16-week old WT or *Osbpl6*$^{-/-}$ mice fed a chow diet (n=3 WT females, n=3 *Osbpl6*$^{-/-}$ females, n=3 WT males, n=3 *Osbpl6*$^{-/-}$ males) were processed in one batch on the same day. For plasma samples, 100µL was used and for brain samples, 40mg of lyophilized total brain sample was used. Extracted samples (1µL of plasma and 0.4 µL of brain) were injected into a 1290 Infinity HPLC coupled to a 6545 accurate mass QTOF MS system (Agilent, Technologies Inc.) equipped with a dual electrospray ionisation (ESI) source and analyzed in both positive and negative ionisation modes. A Zorbax Eclipse plus column (C18, 2.1 x 100 mm, particle size 1.8 µm; Agilent Technologies Inc.) was used for lipid elution using a gradient of solvent A (Methanol/Acetonitrile/Methyl-tert-butyl-ether/Formic acid/Ammonium formate; 55%/35%/10%/0.2%/5mM) or solvent B (Water/Formic acid/Ammonium formate; 100%/0.2%/10mM) over 83 min at 40˚C. MS data processing was achieved using the mass Hunter

Qualitative Analysis software package and an in-house bioinformatic pipeline that we previously developed and described in detail[98]. This data processing yielded a dataset comprising a list of 2296 MS signals or features (lipid entities defined by their mass, retention time and corrected signal intensity) for plasma and 2960 features for brains. Lipid annotation, including FA side chains, was achieved by alignment using our in-house database containing more than 500 lipids previously identified using tandem MS and/or additional tandem MS. The identification of lipids following MS/MS analysis was done by manually interpreting spectra in silico as previously described[100].

2.2.5 Proteomics

Whole brain protein lysates from 16-week old WT or *Osbpl6*$^{-/-}$ mice fed a chow diet (n=5 WT females, n=5 *Osbpl6*$^{-/-}$ females, n=5 WT males, n=5 *Osbpl6*$^{-/-}$ males) were subjected to tryptic digestion and mass spectrometry at the uOttawa Proteomics Resource Center, as previously described[101]. Peptide and protein identifications were obtained using software from the Trans-Proteomic Pipeline (version 6.0.0)[102]. Thermo RAW files were converted using msconvert (version 3)[103]. The database search was performed using Comet (version 2021.01 rev. 0)[104] against the Swiss-Prot *Mus musculus* protein sequences obtained from UniProt[105] (downloaded on 2022-03-29) and their reverse sequences for False Discovery Rate (FDR) assessment. The database search was performed with a precursor ion mass tolerance of 20 ppm, considering fully tryptic peptides with a maximum of 2 miscleavages. Carbamidomethylation of cysteine was considered as a fixed modification and methionine oxidation as a variable modification. Peptide and protein identification confidence was assessed on each sample using PeptideProphet[106], ProteinProphet[107] and iProphet[108]. Peptides and proteins were deemed confidently identified at a FDR < 1%.

2.2.6 Protein differential expression

Protein spectral counts were normalized against the sum of spectral counts in each sample. Student's *t*-tests were performed on normalized protein spectral counts to compare protein quantification in WT and *Osbpl6*$^{-/-}$ mice. A *t*-test was performed if 3 out of 5 samples had

confidently identified the protein in sex specific analyses. Resulting *p*-values were adjusted for multiple hypothesis testing with the Benjamini-Hochberg procedure.

2.2.7 PIGNON analysis

PIGNON[109] was used to identify differentially expressed Gene Ontology (GO) terms when comparing protein quantification in WT versus *Osbpl6*$^{-/-}$ mice and using information contained in a *Mus musculus* protein-protein interaction (PPI) network. PIGNON determined such altered terms using normalized spectral counts from the proteomics analysis and *Mus musculus* PPIs from the BioGRID database[109] (release version 4.4.208) and inferred GO terms from zenodo [DOI: 10.5281/ZENODO.21711]. GO terms annotating between 3 and 1000 proteins were considered by the PIGNON analysis. The weighted Monte Carlo sampling method for statistical assessment was used with a sampling frequency of 100,000. Differentially expressed GO terms were determined at an FDR $\leq$ 1%. As a negative control, a PIGNON analysis was performed on the PPI network without any quantitative data. GO terms that were uniquely identified in the analysis with quantitative data were considered significantly altered. The list of enriched GO terms and their PIGNON-derived *p*-values were submitted to Revigo[110] to summarize the significant terms and provide visualization.

2.2.8 Brain magnetic resonance imaging

For brain imaging, 16-week old WT or *Osbpl6*$^{-/-}$ mice fed a chow diet (n=10 WT females, n=10 *Osbpl6*$^{-/-}$ females, n=10 WT males, n=10 *Osbpl6*$^{-/-}$ males) were anesthetized and transcardially perfused with PBS (Wisent Incorporated, Saint-Jean-Baptiste, Quebec, Canada), gadoteridol (Bracco Diagnostics Incorporated, Monroe Township, New Jersey, USA), and heparin (Sandoz Canada Incorporated, Mississauga, Ontario, Canada) followed by 4% PFA (Electron Microscopy Sciences, Hatfield, Pennsylvania, USA) and gadoteridol in PBS as previously described (Cahill, et al., 2012, Neuroimage; 60:933-9). Skull structures were dissected and post-fixed in 4% PFA and gadoteridol at 4ºC for 12h, after which skulls were transferred into PBS, gadoteridol and sodium trinitride (Fisher Scientific, Mississauga, Ontario, Canada) for storage until scanning. Images were acquired on a 7-Tesla 306 mm horizontal bore magnet (BioSpec 70/30 USR, Bruker, Ettlingen,

Germany) with a ParaVision 6.0.1 console (Zuo et al., 2022 – JCI Insight 7(12):e158144; Arbabi, et al., 2022 – NeuroImage 252:119008). Using a custom-built 8-coil solenoid array, 8 brain samples were imaged in parallel using the following scan parameters: T2W 3D FSE cylindrical k-space acquisition sequence, TR/TE/ETL = 350 ms/12 ms/6, TEeff = 30 ms, four effective averages, FOV/matrix-size = 20.2 x 20.2 x 25.2 mm/504 x 504 x 630. Total imaging time was 13.2 hours with resulting anatomical images of 40µm voxel isotropic resolution. For MRI data analysis, all anatomical brain images were registered together using the mni_autoreg (Collins, et al., 1994 – J. Comput. Assist. Tomogr. 18(2):192-205) and Advanced Normalizations Tools (Avants, et al., 2011 – Neuroimage, 54(3):2033-44) and pydpiper (Friedel, et al., 2014 – Front Neuroinform. 8:67) tool kits. The resulting consensus average and Jacobian determinants were used to quantify volumetric differences between each MRI image and the average. The MAGeT pipeline (Chakravarty, et al., 2013 – Hum. Brain. Mapp. 34(10):2635-2654) was used to segment images using a published classified MRI mouse brain atlas (Dorr et al., 2008 – Neuroimage 42:60-9; Steadmen et al., 2014 – Autism Res. 7:124-137) allowing for volume changes of 182 segmented structures to be calculated. To further assess the effect of genotype on neuroanatomy, an ANOVA was conducted on the log of the jacobian determinants at every voxel with predictors of genotype and sex. All statistics were corrected for multiple comparisons using false-discovery-rate (FDR) (Genovese et al., 2002 – Neuorimage 15, 870-8).

2.2.9 WT vs APP brain samples

Hippocampi of 11-month old WT and APPswe/PSEN1ΔE9 (APPswe) female mice were obtained from the Ferguson Lab at the University of Ottawa. For protein, samples were lysed and homogenized in NP-40 cell lysis buffer (Thermofisher Scientific, FNN0021) with protease inhibitor cocktail (Millipore Sigma, 539134). Samples were incubated on ice for 1hr and spun 2 times at 20000 xg for 10 mins. Supernatants were collected for subsequent protein analysis. For mRNA expression using RT-qPCR, hippocampi were lysed in 500 µL of Trizol and subsequently the RNA was isolated as described below.

2.2.10 Aβ oligomer quantification by ELISA

Quantification was performed as using a sandwich ELISA kit according to manufacturer's instructions, KHB3491 for oligomeric Aβ (Thermo Scientific). Briefly, 50 mg of lyophilized brain protein samples were lysed and centrifuged at 4˚C at 100,000g for 1h. The supernatant was collected and diluted with kit buffer before proceeding with the ELISA as per the manufacturer's protocol. Protein was quantified using the Bradford protein assay. Finally, Aβ concentration was determined upon normalization to total protein concentration.

2.3 Statistical analyses

Experiments were run in triplicates or more in some instances and presented as mean ± SEM. Statistical significance between groups was determined using PRISM Version 9.1.2 software (GraphPad Software Inc). For lipidomics analyses, linear regression without correction for multiple testing was performed. A threshold of $p<0.05$ and fold-change (FC) >1.25 or <0.8 was chosen to select the most discriminant entities between the 2 groups (WT as compared to *Osbpl6*$^{-/-}$) for further validation and identification using MS/MS analysis. P value less than 0.5 were considered statistically significant.

3. RESULTS

3.1 Aim 1: Quantify ORP6 expression in the CNS.

3.1.1 ORP6 expression is abundant in astrocytes in the central nervous system.

Before testing the function of ORP6 in the brain, we first confirmed that its expression is highest in the brain when compared to the other tissues of the body. To do this, we obtained different organs of both male and female C57BL/6J mouse and assessed the expression of ORP6 both at the mRNA and protein levels. Our data reveal that ORP6 is highly enriched in the brain compared to other mouse tissues (**Figure 3a-c**). To gain additional insight on the expression of ORP6 in the brain, we extracted *in situ hybridization* (ISH) data sets from the Allen Brain Atlas[111]. We observed spatial and cell-type-specific expression of ORP6 within the CNS. Amongst the different regions of the mouse brain, we observed the highest ORP6 expression levels in the hippocampal formation (HiF) area, followed by the cortical subplate, pons, medulla and cerebellum (**Figure 3d**) which is consistent with previous data[63]. Moreover, existing mouse and human brain data also demonstrate ORP6 to be highly enriched in astrocytes and neurons as compared to the other cell type of the brain (**Figure 3e-f**). To further define the CNS cell-specificity of ORP6 expression, we next quantified *Osbpl6* mRNA across the following immortalized mouse cell lines: C8-D1A, C8-D30 and C8-S for types I, II and III astrocytes-like cell lines respectively, Neuro-2a for neuron-like cell line and BV2 for microglia. Quantitative real-time PCR (qRT-PCR) revealed significant enrichment of Ospbl6 mRNA in neurons and astrocytes relative to microglia, with the highest expression in type I astrocytes with a 4-fold increase and 41-fold increase to C8-S and C8-D30 respectively (**Figure 3g**). Finally, wild-type (WT) brains were sectioned coronally and stained with ORP6 and the astrocyte marker glial fibrillary acidic protein (GFAP). Immunofluorescent staining revealed a high expression of ORP6 in hippocampus and caudal putamen regions within areas positive for GFAP (**Fig 3h**). Collectively, these results point to an important physiological role for ORP6 in the CNS.

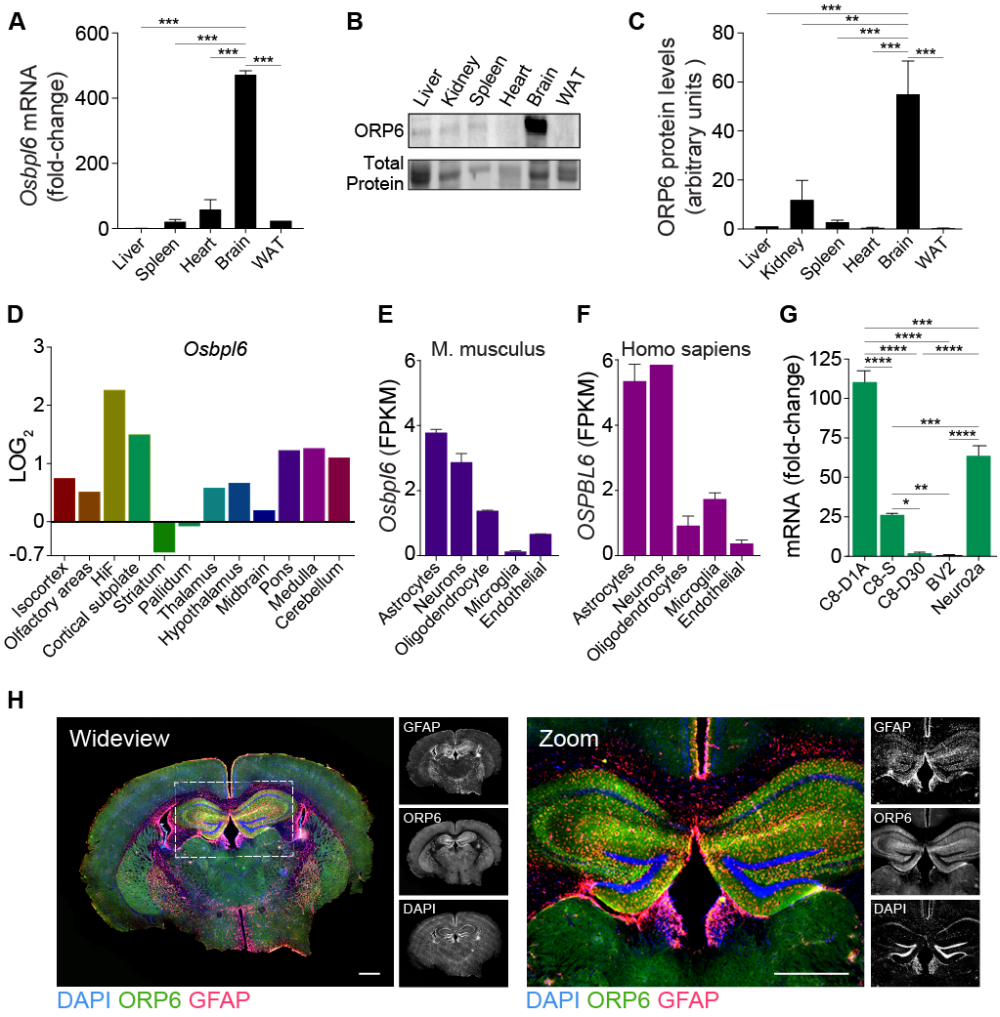

Figure 3. ORP6 is enriched in hippocampal astrocytes.

(**A**) Relative expression of *Osbpl6* in liver, spleen, heart, brain, and white adipose tissue (WAT) of a male C57BL/6J mouse (representative of n=3 males and n=3 females). (**B-C**) ORP6 protein expression, with immunoblotting of ORP6 in mouse tissues shown in (**B**) and densitometry of ORP6 normalized to total protein (**C**). Western blot presented in B is representative of n=3 males and n=3 females and densitometry results are expressed as fold change relative to liver (mean ± SEM, n=3/sex). (**D**) *Osbpl6* gene expression (Log_2 fold-change) in specific brain regions of male C57BL/6J mice by *in situ* hybridization via the Allen Brian Atlas data portal. (**E**, **F**) Enrichment of mouse *Osbpl6* (**E**) and human *OSPBL6* mRNA (**F**) in astrocytes and neurons (brainrnaseq.com). (**G**) qRT-PCR of *Osbpl6* mRNA in murine CNS cell lines. Data is expressed as fold-change for C8-D1A, C8-D30 and C8-S or Neuro-2a cells relative to BV2 cells from one experiment representative of 6 independent experiments with similar results (mean ± sem). (**H**) Representative immunofluorescence staining of GFAP (red) and ORP6 (green) and their colocalization (yellow) in mouse brain sections. n = 5 mice per group. DAPI staining is shown in blue. Scale bar = 1 mm. *P<0.05, **P<0.005, ***P<0.0005, ****P<0.00005.

3.2 Aim 2: Investigating the role of ORP6 in regulating cholesterol homeostasis in CNS cells, in vitro.

3.2.1 ORP6 regulates astrocytic cholesterol biosynthesis and efflux genes.

Given that ORP6 is highly abundant in astrocytes and astrocytes provide most of de novo-synthesized brain cholesterol following oligodendrocytes which are responsible for axon myelinination at early stages of development, [9], we sought to investigate the role of ORP6 in glial cholesterol homeostasis. To identify lipid metabolism genes and pathways regulated by ORP6 in astrocytes, we first knocked down by treating C8-D1A cells with either control or *Osbpl6* siRNA. Knockdown was validated by mRNA and western blot, where *Osbpl6* siRNA was effective in reducing ORP6 mRNA and protein by >80% in these experiments (**Figure 4a**). We then assessed changes in gene expression in both samples by performing gene expression profiling using the Lipoprotein Signaling and Cholesterol Metabolism RT2 Profiler PCR Array containing mouse lipoprotein signals and cholesterol metabolism related gene. Fold change difference between the control and the siRNA treated samples were analysed. Our results indicate that silencing ORP6 in astrocytes led to altered mRNA expression of several genes, where 21 of 84 genes were significantly altered, most notably those involved in cholesterol biosynthesis, cholesterol efflux and cholesterol esterification (**Figure 4b**).

Amongst cholesterol homeostasis genes, upon ORP6 knockdown in astrocytes we observed reduced expression of 7-7-dehydrocholesterol reductase (*Dhcr7*), 3-Hydroxy-3-Methylglutaryl-CoA Synthase 2 (*Hmgcs2*) and Sterol-4-alpha-carboxylate 3-dehydrogenase (*Nsdhl*) (**Figure 4b**). DHCR7 is an enzyme downstream of 3-hydroxy-3-methylglytaryl-CoA reductase (HMGCR) in the cholesterol biosynthesis pathway[11]. HMGCS2 works to catalyze the condensation of acetyl-CoA with acetoacetyl-CoA to form HMG-CoA[112]. NSDHL participates in cholesterol synthesis[113]. Amongst HDL metabolism genes, we observed reduced expression of several apolipoproteins, including *Apod*, *Apof* and *Apol8* and the cholesterol transporter *Abcg1*, in ORP6-silenced astrocytes relative to controls (**Figure 4b**). Notably, ApoD was significantly downregulated with over 50% decrease in expression. Cytochrome P450 heme oxidoreductases cholesterol 7 alpha-hydroxylase (*Cyp7a1*) and oxysterol 7-alpha-hydroxylase (*Cyp7b1*), as well as the lipogenic regulators sterol regulatory element binding proteins 1 and 2 mRNA (*Srebf1*, *Srebf2*), were

downregulated upon ORP6 silencing in astrocytes (**Figure 4b**). In contrast, only two genes were significantly upregulated by ORP6 knockdown related to control: LDL receptor related protein 6 (*Lrp6*) that functions as a regulator of cholesterol homeostasis[114] and sterol O-acyltransferase 1 (*Soat1*) encoding ER-resident ACAT that promotes the formation of cholesterol esters[115] (**Figure 4b)**. Both genes are highly expressed in astrocytes compared to other cells in the brain[64] . These data demonstrate a role for ORP6 in astrocytic cholesterol homeostasis.

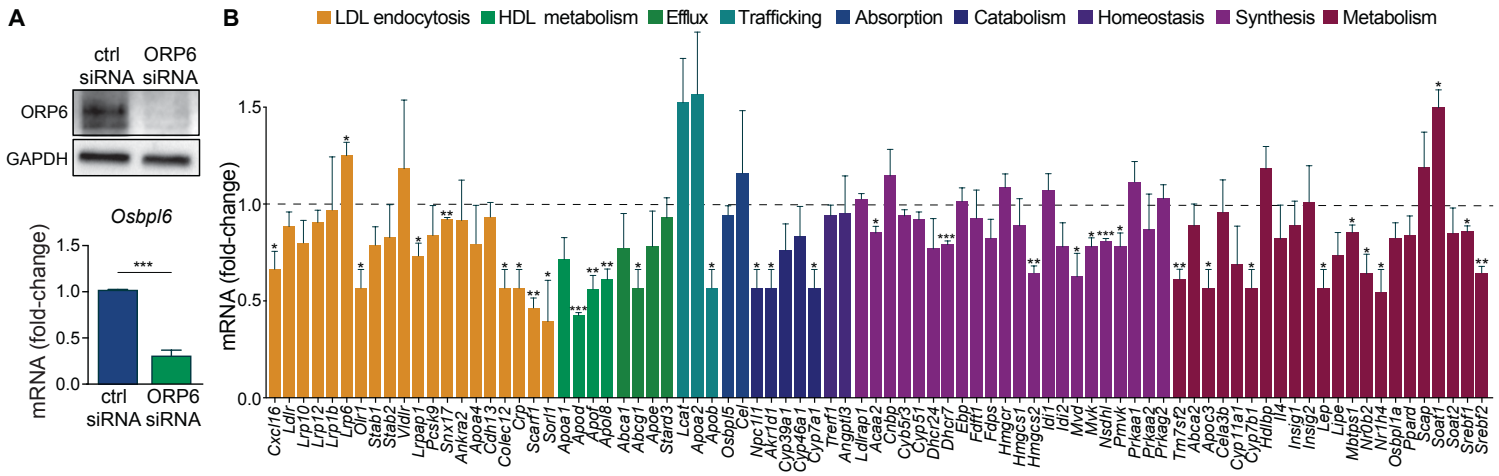

Figure 4. ORP6 regulates cholesterol homeostasis in astrocytes.

(**A**) Immunoblotting of ORP6 and GAPDH (top panel) and qRT-PCR of *Osbpl6* (bottom panel) in C8-D1A astrocytic cells treated with control (ctrl) or *Osbpl6* siRNA. (**B**) qRT-PCR quantification of lipid metabolism genes in astrocytes treated as in (A). Data are displayed as fold-change of ORP6 siRNA-treated C8-D1A cells relative to ctrl siRNA-treated cells of 3 independent experiments (mean±SEM). *P<0.05, ***P*<0.005, ****P*<0.0005 by Student's t-test.

3.2.2 ORP6 knockdown promotes lipid droplet accumulation and reduces cholesterol efflux.

To further elucidate the role of ORP6 in astrocyte cholesterol homeostasis, we next incubated C8-D1A cells with 100µg/mL of methyl-beta-cyclodextrin (mβ-CD)-cholesterol complexes for 24h to lipid-load these with cholesterol. As compared to unloaded cells, lipid-loaded astrocytes showed an increase in the formation of cytosolic LDs (**Figure 5a**). This was accompanied by a 3-fold increase in ORP6 expression at the mRNA and protein levels (**Figure 5b** and **5a** respectively). Reduced ORP6 expression by ORP6 knockdown in unloaded or cholesterol-loaded C8-D1A cells was confirmed by immunofluorescent staining and quantification (**Figure 5c**). In parallel, we observed that transfecting the C8-D1A cells with ORP6 siRNA resulted in a marked increase in neutral lipids and free cholesterol compared to control siRNA-treated cells, as detected by BODIPY and filipin staining, respectively (**Figure 5d**). Additional IF studies showed increased levels of cytosolic LDs in ORP6 siRNA-treated cells relative to control, in both unloaded and cholesterol-loaded conditions (**Figure 5e**). Increased accumulation of astrocytic LDs upon ORP6 knockdown was associated with elevated mRNA expression of the structural LD protein perilipin 2 (*Plin2*) (**Figure 5f**) and elevated expression of *Soat1/Acat1* mRNA (**Figure 5g)** by qRT-PCR. Increased expression of PLIN2 and SOAT1/ACAT1, was confirmed at the protein level by western blot analysis (**Figure 5h**).

To directly test if ORP6 silencing increased cholesterol esterification in astrocytes, we pulsed control or ORP6 siRNA-treated C8-D1A cells with ^{3}H-cholesterol and subsequently quantified its incorporation into ^{3}H-cholesterol esters by TLC. Knockdown of ORP6 resulted in a two-fold increase in ^{3}H-cholesterol esters (**Figure 5i**). As cholesterol is accumulating within astrocytes by conversion into CE, we then sought to determine the effect of ORP6 knockdown in astrocyte cholesterol efflux. After labelling C8-D1A cells with ^{3}H-cholesterol, cholesterol acceptors, HDL and apo-A1 were added to the cells for 6 hrs. ORP6 silencing reduced efflux reduced ^{3}H-cholesterol efflux to both HDL (**Figure 5j**) and lipid-poor apolipoprotein A-I (apoA-I) (**Figure 5k**). The observed effect on cholesterol efflux was not as pronounced as expected, and this could be partly explained by the fact that the silencing of ORP6 is variable across experiments. Nevertheless, our data aligns with previously reported effects in macrophages[61].

Thus, taken together, our results indicate that ORP6 is regulated by cholesterol levels in astrocytes and establishes a role for ORP6 in the esterification and accumulation of cholesterol in cytosolic LDs.

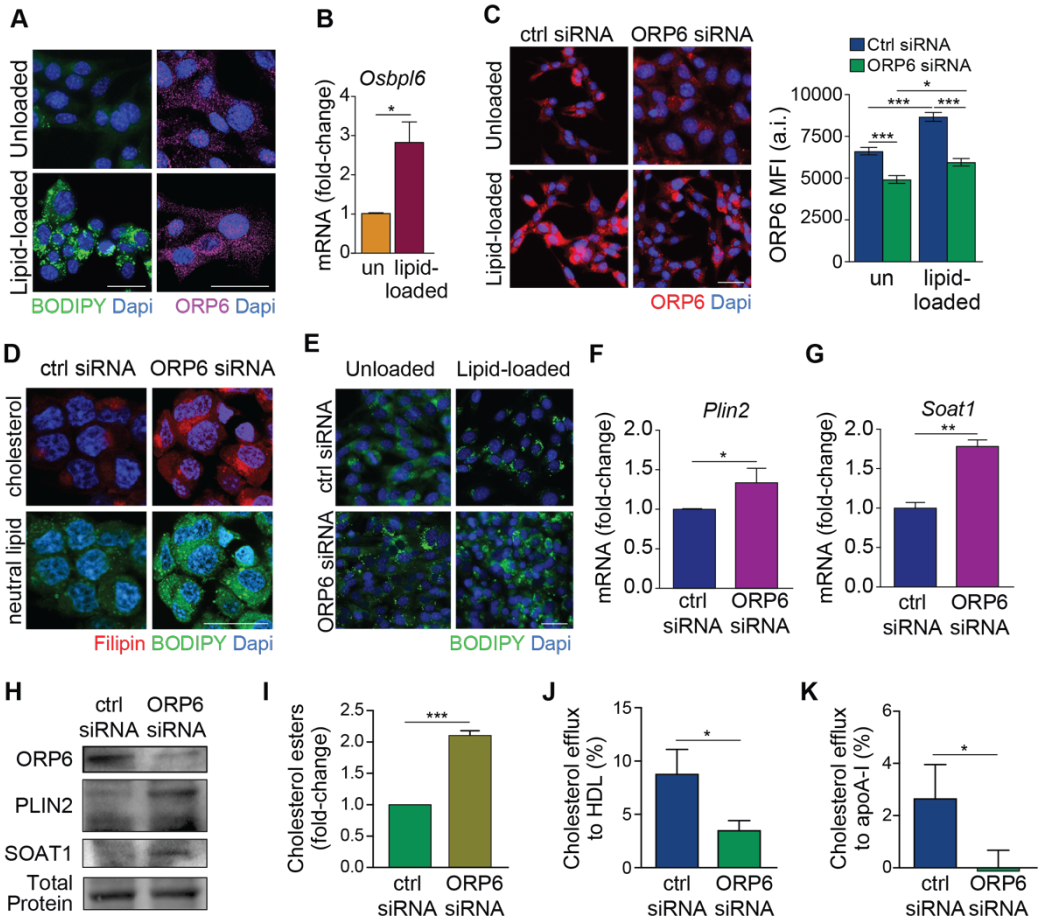

Figure 5. ORP6 promotes lipid droplet accumulation and reduces cholesterol efflux.
(A) Immunofluorescence (IF) staining for BODIPY (green), ORP6 (magenta) and DAPI (blue) in C8-D1A astrocytes treated with 100µg/mL of methyl-beta-cyclodextrin (mβ-CD)-cholesterol complexes for 24h (lipid-loaded) as compared to unloaded. (**B**) qRT-PCR of *Osbpl6* mRNA in C8-D1A cells treated as in (C) (n=3). (**C**) IF staining for ORP6 (red) and DAPI (blue) in C8-D1A astrocytic cells treated with control (ctrl) or ORP6 siRNA lipid-loaded as in (A) as compared to unloaded. Quantification of ORP6 mean fluorescence intensity (MFI) shown at right. a.i. = arbitrary units. (**D**) IF staining for BODIPY (green), Filipin (red) and DAPI (blue) in C8-D1A astrocytes treated with ctrl siRNA or ORP6 siRNA. (**E**) IF staining for BODIPY (green) and DAPI (blue) in C8-D1A astrocytes treated as in (E). (**F**, **G**) qRT-PCR of *Plin2* and *Soat1* mRNA in ORP6 as compared to ctrl siRNA-treated C8-D1A cells (n=5). (**H**) Immunoblotting of ORP6, PLIN2, SOAT1 in C8-D1A cells transfected with ctrl or ORP6 siRNA. Image is representative of n=4 independent experiments. (**I**) Relative cholesterol esters as quantified by thin layer chromatography of C8-D1A cells transfected with ctrl or ORP6 siRNA and loaded with ^{3}H-cholesterol for 24hr (n=3) and effluxed to BSA. (**J**, **K**) ^{3}H-cholesterol efflux to HDL (**J**) or apoA-1 (**K**) for 4 hrs in ctrl or ORP6 siRNA-treated C8-D1A cells. Data is expressed as representative of 4 independent experiments with similar results (n=4). Scale bar = 25 µm. (A-K) Data shown is mean ± SEM; *P<0.05, ***P*<0.005, ****P*<0.0005 by Student's T-test.

3.3 Aim 3: Investigate the role of ORP6 in whole body lipid homeostasis, in vivo.

3.3.1 ORP6 ablation results in altered plasma lipids.

To gain insight into the function of ORP6 *in vivo*, we generated *Osbpl6* deficient (*Osbpl6*$^{-/-}$) mice at The Centre for Phenogenomics (TCP) using CRISPR/Cas9 gene targeting technology to knock out ORP6 expression in C57BL6/N mice (**Figure 2)**. Successful knockout of ORP6 expression in our mice was confirmed by Western blot protein analysis of tissues of wild-type (WT) and *Osbpl6*$^{-/-}$ (**Figure 6a**). The analysis also further confirmed the significantly higher expression of ORP6 in the brain compared to the other organs (**Figure 6a**). Initial assessment reveal that *Osbpl6*$^{-/-}$ mice were viable and fertile with no apparent gross tissue abnormalities or specific changes in body weights (**Suppl. Figure 1**). For mouse viability, from *Osbpl6*$^{+/-}$ mice heterozygous crosses, we obtained 129 males (48%) and 141 females (52%). Amongst females we obtained 33 WT, 68 *Osbpl6*$^{+/-}$ and 40 *Osbpl6*$^{-/-}$ mice, and amongst males we obtained 41 WT, 68 *Osbpl6*$^{+/-}$ and 20 *Osbpl6*$^{-/-}$ mice (**Figure 6b**).

To investigate whether ORP6 deficiency alters in lipid metabolism, we performed unbiased untargeted lipidomic analysis of plasma from 16-week-old male and female WT and *Osbpl6*$^{-/-}$ mice. We observed that 470 MS signal features were significantly distinct between WT and *Osbpl6*$^{-/-}$ mice, from which we identified 40 unique lipids using MS/MS analysis and an additional 54 using an in-house database (**Table 4**). Of the different lipid classes observed to be differentially abundant in *Osbpl6*$^{-/-}$ mice as compared to WT, such as free fatty acids (FFA), acylcarnitines (AC), cholesterol esters (CE), diacylglycerols (DG) and triacylglycerols (TG), amongst others (**Figure 6c** and **Table 4**), we observed enhanced plasma levels of some TG, DG and PC species, particularly those enriched with 18:2 acyl chains, concomitant with a downregulation of a few cholesterol esters and several subspecies of LPCs, PCs and PIs typically enriched in high density lipoprotein (HDL) particles [116] (**Figure 6d**). We observed no differences among the groups in plasma total TG levels (**Figure 6e**). However, both plasma total cholesterol levels and plasma HDL-cholesterol was significantly reduced in male *Osbpl6*$^{-/-}$ mice relative to WT (**Figure 6f** and **6g**), consistent with previous reports which observed a correlation between ORP6 and plasma HDL-cholesterol levels[61].

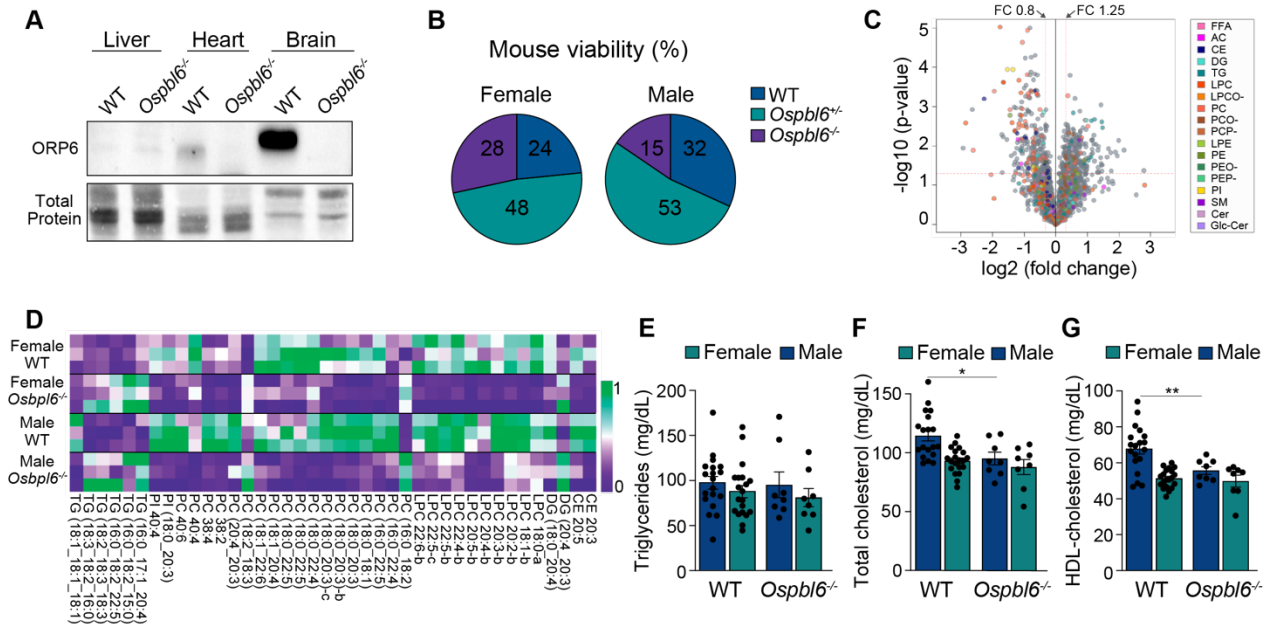

Figure 6. Loss of ORP6 in mice alters plasma lipid and lipoprotein profiles.

(A) Immunoblotting of ORP6 and Total protein in different organs of wild-type (WT) and *Osbpl6*$^{-/-}$ mice. **(B)** Mouse viability of WT, *Osbpl6*$^{+/-}$ and *Osbpl6*$^{-/-}$ represented as percentage of total obtained mice from heterozygous crosses. **(C)** Volcano plot of altered lipid species in the plasma of *Osbpl6*$^{-/-}$ mice vs WT mice. Data represented as the log2 fold change (FC) of *Osbpl6*$^{-/-}$ vs. WT group was plotted against the -log10 p-value. Statistical significance was evaluated by t-test (p-value < 0.05) and FC threshold was set to lower than 0.8 and higher than 1.5 (n=6 per genotype). Colored entities represent lipid species that are significantly dysregulated divided by lipid (sub)classes (**D**) Heatmap representing significantly different entities annotated by MS/MS normalized to the area under the curve between WT and *Osbpl6*$^{-/-}$ mice (n=3 per genotype per sex). **(E)** Triglyceride, **(F)** Total cholesterol, and **(G)** HDL cholesterol levels in wild-type (WT) and *Osbpl6*$^{-/-}$ mice stratified by sex. (n=18-19 for WT and n=9 for *Osbpl6*$^{-/-}$ per sex). *P<0.05, **P<0.005 by one-way ANOVA with Tukey's multiple comparisons test (E-G).

Table 4. Plasma MS signal entities identified by using MS/MS analysis and the Montreal Heart Institute Metabolomic platform internal database.

Compound Name	Lipid ID	P value	FC	Change	Annotation	Compound Name	Lipid ID	P value	FC	Change	Annotation
Pos:631.5179@27.08	DG(18:2_18:3)	0.002	1.95	up	MS/MS	Pos:769.5628@22.30	PC(17:1_18:2)	0.008	1.58	up	Internal database
Pos:757.5678@23.45	PC(16:0_18:2)	0.035	1.30	up	MS/MS	Pos:863.6405@30.53	PC(18:0_24:5)	0.040	1.32	up	Internal database
Pos:779.5473@19.27	PC(18:2_18:3)	0.003	2.02	up	MS/MS	Pos:781.5641@21.45	PC(18:2_18:2)	0.042	1.55	up	Internal database
Pos:883.7635@51.60	TG(16:0_17:1_20:4)	0.002	1.47	up	MS/MS	Pos:845.6881@38.30	PC(40:0)	0.015	1.71	up	Internal database
Pos:833.7477@52.41	TG(16:0_18:2_15:0)	0.002	2.34	up	MS/MS	Pos:739.5522@21.44	PC(O-14:0/20:4)	0.005	1.45	up	Internal database
Pos:921.7798@51.24	TG(16:0_18:2_22:5)	0.002	2.18	up	MS/MS	Pos:719.5834@28.03	PC(O-16:0/16:0)	0.018	1.43	up	Internal database
Pos:891.7325@42.76	TG(18:2_18:3_18:3)	0.003	2.74	up	MS/MS	Pos:747.6150@32.40	PC(O-16:0/18:0)	0.020	1.51	up	Internal database
Pos:869.7488@48.16	TG(18:3_18:2_16:0)	0.004	2.79	up	MS/MS	Pos:771.6148@29.88	PC(O-18:0/18:2)	0.031	1.27	up	Internal database
Pos:691.6263@57.00	CE(20:3)	0.037	0.21	down	MS/MS	Pos:795.6147@29.31	PC(O-18:0/20:4)	0.021	1.25	up	Internal database
Pos:692.5514@47.25	CE(20:5)	0.035	0.63	down	MS/MS	Pos:717.5677@27.37	PC(P-16:0/16:0)	0.005	1.33	up	Internal database
Pos:626.5288@22.38	DG(18:0_20:4)	0.001	0.77	down	MS/MS	Pos:747.5784@34.53	PE(18:0_18:0)	0.043	1.50	up	Internal database
Pos:523.3649@10.74	LPC(18:0)	0.003	0.48	down	MS/MS	Pos:743.5493@27.65	PE(18:1_18:1)	0.048	1.58	up	Internal database
Pos:521.3496@9.79	LPC(18:1)	0.004	0.41	down	MS/MS	Pos:739.5170@22.07	PE(18:2_18:2)	0.023	1.88	up	Internal database
Pos:547.3644@10.30	LPC(20:2)	0.003	0.45	down	MS/MS	Pos:789.5300@27.65	PE(22:6_18:1)	0.022	1.47	up	Internal database
Pos:545.3489@9.26	LPC(20:3)	0.030	0.32	down	MS/MS	Pos:725.5373@26.01	PE(O-16:0/20:4)	0.021	1.54	up	Internal database
Pos:543.3338@8.47	LPC(20:4)	0.035	0.47	down	MS/MS	Pos:777.5679@29.10	PE(O-18:0/22:6)	0.028	1.32	up	Internal database
Pos:541.3171@7.32	LPC(20:5)	0.009	0.29	down	MS/MS	Pos:814.6939@36.28	SM(d18:1/24:0)	0.007	1.67	up	Internal database
Pos:571.3639@9.98	LPC(22:4)	0.029	0.45	down	MS/MS	Pos:781.7162@51.29	TG(45:0)	0.032	1.40	up	Internal database
Pos:569.3484@8.96	LPC(22:5)	0.003	0.38	down	MS/MS	Pos:876.7201@51.54	TG(52:4)	0.011	1.34	up	Internal database
Pos:569.3489@9.45	LPC(22:5)	0.030	0.32	down	MS/MS	Pos:867.7324@45.21	TG(52:6)	0.023	2.03	up	Internal database
Pos:567.3335@8.41	LPC(22:6)	0.002	0.47	down	MS/MS	Pos:900.7193@49.67	TG(54:6)	0.008	1.42	up	Internal database
Neg:855.5967@25.92	PC(16:0_22:4)	0.004	0.53	down	MS/MS	Pos:895.7651@48.00	TG(54:6)	0.029	1.87	up	Internal database
Neg:853.5812@24.65	PC(16:0_22:5)	0.009	0.54	down	MS/MS	Pos:893.7482@45.05	TG(54:7)	0.019	2.16	up	Internal database
Neg:833.6130@30.33	PC(18:0_18:1)	0.035	0.55	down	MS/MS	Pos:425.3508@9.37	18:1 carnitine	0.007	2.30	down	Internal database
Neg:857.6129@28.54	PC(18:0_20:3)	0.013	0.48	down	MS/MS	Pos:423.3353@8.15	18:2 carnitine	0.029	2.14	down	Internal database
Pos:811.6112@28.60	PC(18:0_20:3)	0.025	0.53	down	MS/MS	Pos:639.5967@53.98	CE(16:1)	0.037	1.82	down	Internal database
Pos:811.6098@29.69	PC(18:0_20:3)	0.035	0.26	down	MS/MS	Pos:691.6278@55.73	CE(20:3)	0.006	1.92	down	Internal database
Pos:837.6253@29.88	PC(18:0_22:4)	0.035	0.67	down	MS/MS	Pos:602.5274@35.53	DG(18:1/18:1)	0.018	1.49	down	Internal database
Neg:881.6130@28.54	PC(18:0_22:5)	0.035	0.58	down	MS/MS	Pos:507.3691@10.47	LPC(O-18:1)	0.042	1.63	down	Internal database
Pos:835.6097@28.59	PC(18:0_22:5)	0.035	0.55	down	MS/MS	Pos:523.3662@11.09	LPC(18:0)	0.040	1.55	down	Internal database
Neg:853.5816@23.65	PC(18:1_20:4)	0.001	0.70	down	MS/MS	Pos:519.3341@8.52	LPC(18:2)	0.021	1.61	down	Internal database
Neg:877.5816@22.89	PC(18:1_22:6)	0.035	0.66	down	MS/MS	Pos:481.3173@11.25	LPE(18:0)	0.036	1.51	down	Internal database
Pos:817.6583@36.36	PC(20:4_20:3)	0.002	0.51	down	MS/MS	Pos:779.5479@20.88	PC(16:0_20:5)	0.024	1.65	down	Internal database
Neg:859.6283@31.12	PC(38:2)	0.001	0.48	down	MS/MS	Pos:809.5942@25.95	PC(16:0_22:4)	0.016	1.65	down	Internal database
Neg:855.5965@25.27	PC(38:4)	0.004	0.44	down	MS/MS	Pos:807.5791@24.69	PC(16:0_22:5)	0.006	1.66	down	Internal database
Neg:883.6276@29.82	PC(40:4)	0.004	0.65	down	MS/MS	Pos:757.5633@23.16	PC(16:1_18:1)	0.013	6.12	down	Internal database
Pos:833.5937@25.34	PC(40:6)	0.001	0.37	down	MS/MS	Pos:787.6113@30.40	PC(18:0_18:1)	0.019	1.31	down	Internal database
Pos:719.5482@30.39	PI(18:0_20:3)	0.025	0.35	down	MS/MS	Pos:813.6254@31.18	PC(18:0_20:2)	0.008	1.62	down	Internal database
Neg:914.5853@24.94	PI(40:4)	0.025	0.39	down	MS/MS	Pos:835.6106@27.28	PC(18:0_22:5)	0.022	1.41	down	Internal database
Pos:901.8119@65.36	TG(18:1_18:1_18:1)	0.013	0.46	down	MS/MS	Pos:785.5953@26.96	PC(18:1_18:1)	0.014	1.62	down	Internal database
Pos:649.6381@38.77	Cer(d18:1/24:0)	0.012	1.43	up	Internal database	Pos:809.5945@25.30	PC(18:1_20:3)	0.007	2.09	down	Internal database
Pos:649.4688@15.57	PC(12:0_14:0)	0.024	1.55	up	Internal database	Pos:807.5799@23.69	PC(18:1_20:4)	0.022	1.25	down	Internal database
Pos:677.5014@18.36	PC(14:0_14:0)	0.006	1.77	up	Internal database	Pos:831.5798@22.94	PC(18:1_22:6)	0.006	1.36	down	Internal database
Pos:743.5472@21.68	PC(15:0_18:2)	0.028	1.52	up	Internal database	Pos:831.5784@22.08	PC(20:4_20:3)	0.027	1.88	down	Internal database
Pos:767.5471@21.27	PC(15:0_20:4)	0.031	1.29	up	Internal database	Pos:855.5779@20.97	PC(20:4_22:5)	0.022	1.80	down	Internal database
Pos:719.5470@23.70	PC(16:0_15:0)	0.006	1.46	up	Internal database	Pos:929.5988@22.77	PI(18:0_22:5)	0.034	1.63	down	Internal database
Pos:779.5450@23.59	PC(16:0_18:2)	0.045	1.27	up	Internal database	Pos:901.8119@65.36	TG(54:3)	0.013	2.16	down	Internal database

3.3.2 ORP6 ablation alters circulating brain lipids and Aβ deposition.

Because the blood-brain-barrier is impermeable to lipoproteins, preventing blood cholesterol from reaching the brain, cholesterol levels and trafficking in the brain are uniquely regulated by endogenous mechanisms[18]. We employed unbiased lipidomics to examine the brain lipid profiles of *Osbpl6*$^{-/-}$ mice as compared to WT mice. We observed that 114 brain MS signal features were distinct between WT and *Osbpl6*$^{-/-}$ mice, from which we identified 51 unique lipids using MS/MS analysis (p-value < 0.05 with fold change threshold set to lower than 0.8 and higher than 1.5), including several glycerophospholipids (GPL) and glycerolipids (GL) (**Figure 7a**, **7b** and **Table 5**). Notably, 3 diacylglycerol (DG) species were elevated in male and female *Osbpl6*$^{-/-}$ brains while 13 TG species were reduced (**Figure 7a**). Intriguingly, within the cholesterol biosynthesis pathway, only the intermediate desmosterol was uniquely elevated in the brains of *Osbpl6*$^{-/-}$ mice relative to WT (**Figure 7c**), while total cholesterol levels remained unchanged (**Figure 7d**).

Non-cholesterol sterols in the CNS are associated with AD, amyloid pathology and cognitive decline, and desmosterol has emerged as an early biomarker of AD[19]. As such, we next employed quantitative proteomics to detect differentially expressed proteins in the brains of *Osbpl6*$^{-/-}$ mice relative to WT. Unexpectedly, our proteomics results identified a single protein as significantly altered between the WT and *Osbpl6*$^{-/-}$ mice : neuroligin-1 (NLGN1), a postsynaptic cell adhesion protein critical for synaptic function[117,118] (**Figure 8a**). Using PIGNON[109] to identify cell processes differentially expressed in *Osbpl6*$^{-/-}$ and WT mice, we found 42 gene ontology (GO) terms to be dysregulated, including behavior and learning, synapse organization and plasticity, and organelle localization within the biological processes (**Figure 8b**). Altered cell components and molecular functions in *Osbpl6*$^{-/-}$ and WT mice included main axon and glutamate receptor activities (**Figure 8b**). Notable proteins comprising these pathways include: amyloid precursor protein (APP), the a disintegrin and metalloproteinase (ADAM) protein family that possesses α-secretase APP cleavage activity, presenilins 1 and 2 that are the catalytic subunits of APP-cleaving γ-secretase, brain-derived neurotrophic factor (BDNF) that is an important trophic factor active in the hippocampus, cortex and basal forebrain supporting neuron survival and playing a pivotal

role in synaptic plasticity and cognition in AD, the afore-mentioned NLGL1 and all the glutamate receptors that play a key role in memory and in AD pathogenesis (**Table 6**).

As previously mentioned, the hallmark of AD is the accumulation of Aβ and NFTs[69]. The oligomeric form of Aβ is the most neurotoxic, whereby its buildup leads to the insoluble and aggregated amyloid plaques[69]. Given that multiple GO terms, cell components and molecular functions and players linked to Aβ processing were shown to be altered in the *Osbpl6*$^{-/-}$ compared to WT by the proteomics analysis, along with the known role for Aβ-regulated NLGN1 in driving synaptotoxicity in AD[118], we next quantified Aβ levels in our mice. Quantification of soluble Aβ oligomers (sAβ) by ELISA of the brain homogenates from WT and *Osbpl6*$^{-/-}$ mice revealed a significant 1.4-fold increase in sAβ in *Osbpl6*$^{-/-}$ mice compared to WT (**Figure 8c**). Collectively, the lipidomics results along with the identification of several altered pathways related to AD and increased soluble Aβ, suggests a novel role for ORP6 in the pathogenesis of AD.

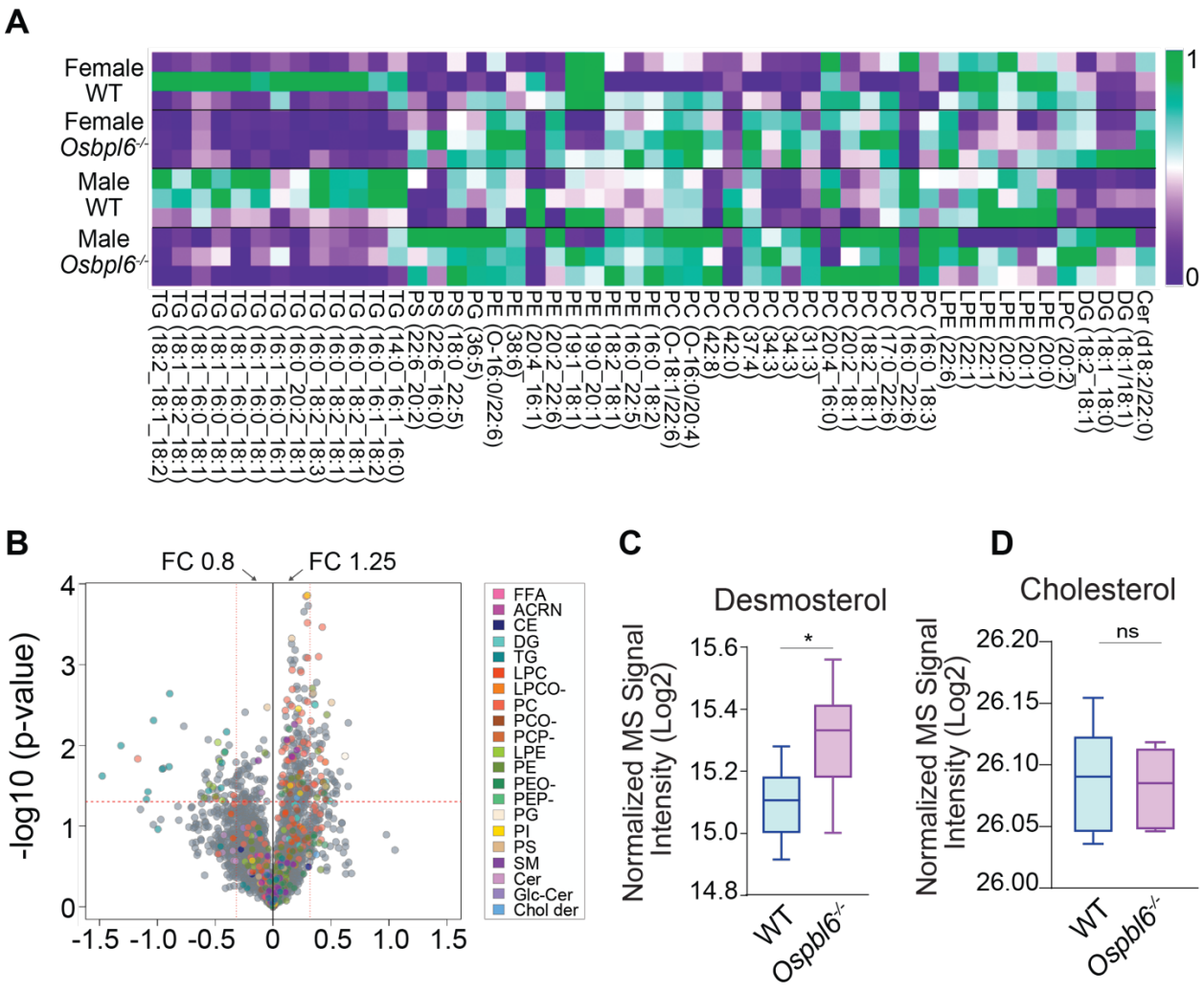

Figure 7. Loss of ORP6 in mice alters CNS lipid species.

(**A**) Heatmap of significantly altered brain lipid species annotated by MS/MS normalized to the area under the curve between WT and *Osbpl6*$^{-/-}$ mice (n=3 per genotype / sex). **(B)** Volcano plot of altered lipid species in the brain of *Osbpl6*$^{-/-}$ mice vs WT mice. Data represented as the log2 fold change (FC) of *Osbpl6*$^{-/-}$ vs. WT group was plotted against the -log10 p-value. Statistical significance was evaluated by t-test (p-value < 0.05) and FC threshold was set to lower than 0.8 and higher than 1.5 (n=6 per genotype / sex). Colored entities represent lipid species that are significantly dysregulated divided by lipid (sub)classes (**B**) (**C-D**) Normalized MS signal intensity (Log 2) of desmosterol (C) and cholesterol (D) (mean± SEM, n=6 per genotype). P<0.05 by Student's t-test.

Table 5. Brain MS signal entities identified using MS/MS analysis.

Compound Name	Lipid ID	P value	FC	Change	Annotation
Pos:619.5921@35.06	Cer(d18:2/22:0)	0.031	1.27	up	MS/MS
Pos:637.5656@35.74	DG(18:1/18:1)	0.028	1.37	up	MS/MS
Pos:639.5809@37.22	DG(18:1_18:0)	0.049	1.40	up	MS/MS
Pos:635.5495@32.97	DG(18:2_18:1)	0.003	1.29	up	MS/MS
Pos:547.3644@9.94	LPC(20:2)	0.016	1.37	up	MS/MS
Pos:525.2858@24.46	LPE(22:6)	0.028	1.35	up	MS/MS
Pos:755.5470@21.10	PC(16:0_18:3)	0.038	1.34	up	MS/MS
Pos:819.5781@24.27	PC(17:0_22:6)	0.030	1.28	up	MS/MS
Pos:783.5788@24.19	PC(18:2_18:1)	0.015	1.33	up	MS/MS
Pos:811.6085@27.74	PC(20:2_18:1)	0.030	1.28	up	MS/MS
Pos:713.5003@21.12	PC(31:3)	0.011	1.33	up	MS/MS
Pos:755.5465@25.24	PC(34:3)	0.000	1.34	up	MS/MS
Pos:755.5469@21.67	PC(34:3)	0.001	1.31	up	MS/MS
Pos:795.5785@24.53	PC(37:4)	0.024	1.33	up	MS/MS
Pos:857.5940@23.72	PC(42:8)	0.005	1.25	up	MS/MS
Pos:767.5832@25.27	PC(O-16:0/20:4)	0.028	1.35	up	MS/MS
Pos:817.5976@24.98	PC(O-18:1/22:6)	0.047	1.37	up	MS/MS
Pos:715.5160@24.19	PE(16:0_18:2)	0.012	1.31	up	MS/MS
Pos:765.5346@25.38	PE(16:0_22:5)	0.044	1.30	up	MS/MS
Pos:741.5318@24.82	PE(18:2_18:1)	0.032	1.38	up	MS/MS
Pos:815.5514@24.36	PE(20:2_22:6)	0.004	1.38	up	MS/MS
Pos:763.5176@22.06	PE(38:6)	0.002	1.27	up	MS/MS
Pos:749.5369@25.16	PE(O-16:0/22:6)	0.039	1.36	up	MS/MS
Pos:785.5209@21.24	PG(36:5)	0.013	1.54	up	MS/MS
Pos:837.5515@24.33	PS(18:0_22:5)	0.032	1.37	up	MS/MS
Pos:807.5054@19.80	PS(22:6_16:0)	0.003	1.42	up	MS/MS
Pos:859.5358@21.03	PS(22:6_20:2)	0.002	1.27	up	MS/MS
Neg:509.3480@12.43	LPE(20:0)	0.012	0.75	down	MS/MS
Neg:507.3334@11.22	LPE(20:1)	0.009	0.72	down	MS/MS
Neg:505.3165@10.28	LPE(20:2)	0.048	0.74	down	MS/MS
Neg:535.3635@12.64	LPE(22:1)	0.015	0.72	down	MS/MS
Neg:535.3634@13.01	LPE(22:1)	0.032	0.70	down	MS/MS
Pos:827.5447@22.27	PC(16:0_22:6)	0.015	0.44	down	MS/MS
Neg:891.6911@38.01	PC(24:0_16:0)	0.046	0.71	down	MS/MS
Pos:873.7189@40.25	PC(42:0)	0.041	0.79	down	MS/MS
Neg:787.6075@33.02	PE(19:0_20:1)	0.030	0.68	down	MS/MS
Neg:759.5766@29.15	PE(19:1_18:1)	0.043	0.71	down	MS/MS
Pos:737.4996@20.74	PE(20:4_16:1)	0.045	0.66	down	MS/MS
Pos:793.7162@49.82	TG(14:0_16:1_16:0)	0.016	0.74	down	MS/MS
Pos:845.7479@50.83	TG(16:0_16:1_18:2)	0.024	0.36	down	MS/MS
Pos:873.7790@57.16	TG(16:0_18:2_18:1)	0.019	0.52	down	MS/MS
Pos:869.7473@47.70	TG(16:0_18:2_18:3)	0.047	0.47	down	MS/MS
Pos:906.7655@65.36	TG(16:0_20:2_18:1)	0.002	0.54	down	MS/MS
Pos:819.7316@50.49	TG(16:1_16:0_16:1)	0.036	0.68	down	MS/MS
Pos:847.7634@56.23	TG(16:1_16:0_18:1)	0.018	0.53	down	MS/MS
Pos:897.7785@51.95	TG(18:1_16:0_18:1)	0.037	0.47	down	MS/MS
Pos:875.7946@64.66	TG(18:1_16:0_18:1)	0.033	0.73	down	MS/MS
Pos:899.7949@57.68	TG(18:1_18:2_18:1)	0.010	0.40	down	MS/MS
Pos:880.7502@64.71	TG(18:2_18:1_18:2)	0.012	0.75	down	MS/MS

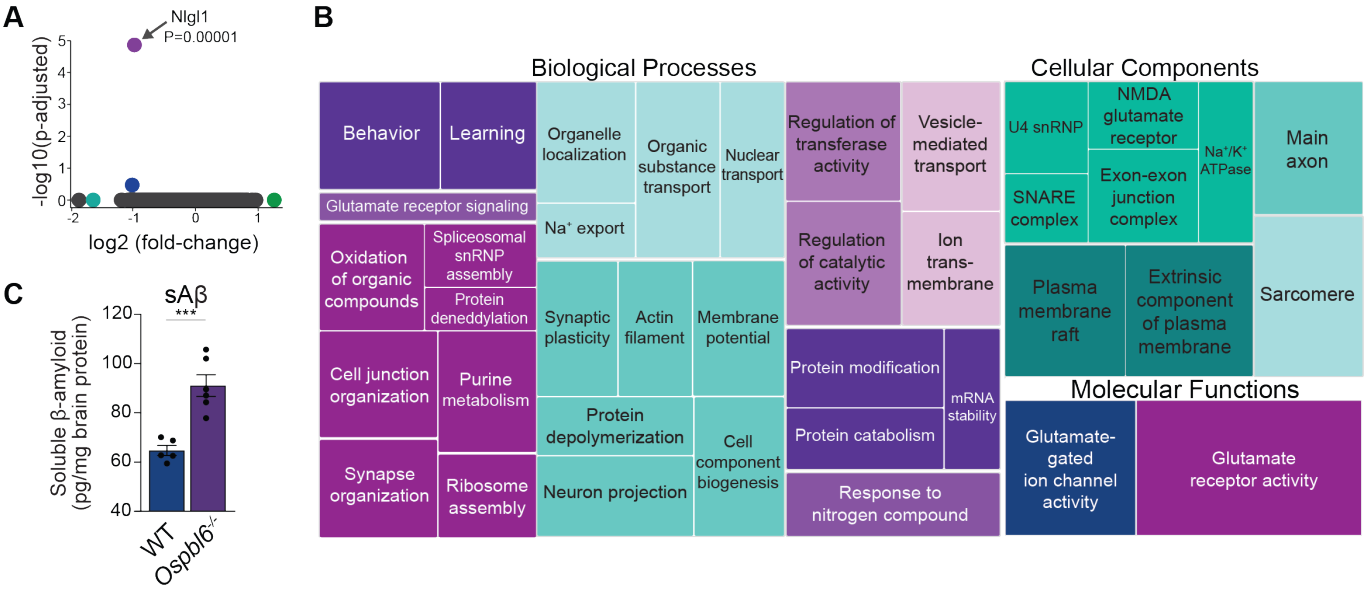

Figure 8. Loss of ORP6 in mice alters biological processes and increases Aβ deposition.
(**A**) Volcano plot of altered protein expression in male WT and *Osbpl6*$^{-/-}$ brains as quantified by unbiased proteomics analysis. Data represented as the log2 fold change of *Osbpl6*$^{-/-}$ vs. WT group plotted against the -log10 adjusted p-value (p-adjusted) (n=5 per genotype). (**B**) Treemap of altered biological processes, cellular components, and molecular functions in WT and *Osbpl6*$^{-/-}$ brains as quantified by unbiased proteomics analysis using PIGNON (n=5 per genotype / sex). (**C**) Whole brain Aβ oligomer concentrations (pg/mg protein) in age-matched WT and *Osbpl6*$^{-/-}$ mice at 16 weeks (n=5 per genotype / sex, mean ± SEM). *P<0.05, **P<0.005, ***P<0.0005.

Table 6. Altered biological processes, cell components and molecular functions in WT and *Osbpl6*$^{-/-}$ brains.

ID	Name	Category	P-value	FDR
GO:0000338	protein deneddylation	biological_process	3.07E-07	0.005607
GO:0000387	spliceosomal snRNP assembly	biological_process	4.05E-07	0.005607
GO:0005234	extracellular-glutamate-gated ion channel activity	molecular_function	4.60E-07	0.005607
GO:0005687	U4 snRNP	cellular_component	1.47E-07	0.005607
GO:0005890	sodium:potassium-exchanging ATPase complex	cellular_component	4.88E-07	0.005607
GO:0007612	learning	biological_process	3.73E-07	0.005607
GO:0008066	glutamate receptor activity	molecular_function	1.40E-07	0.002273
GO:0010975	regulation of neuron projection development	biological_process	3.09E-07	0.005607
GO:0015980	energy derivation by oxidation of organic compounds	biological_process	3.86E-07	0.005607
GO:0017146	NMDA selective glutamate receptor complex	cellular_component	4.76E-07	0.005607
GO:0019897	extrinsic component of plasma membrane	cellular_component	3.10E-07	0.005607
GO:0030017	sarcomere	cellular_component	5.72E-07	0.005607
GO:0030833	regulation of actin filament polymerization	biological_process	2.28E-07	0.005607
GO:0031400	negative regulation of protein modification process	biological_process	3.22E-07	0.005607
GO:0031674	I band	cellular_component	5.06E-07	0.005607
GO:0032412	regulation of ion transmembrane transporter activity	biological_process	4.40E-07	0.005607
GO:0034330	cell junction organization	biological_process	6.22E-07	0.005607
GO:0035145	exon-exon junction complex	cellular_component	5.72E-07	0.005607
GO:0035235	ionotropic glutamate receptor signaling pathway	biological_process	8.93E-08	0.002273
GO:0036376	sodium ion export from cell	biological_process	4.88E-07	0.005607
GO:0042255	ribosome assembly	biological_process	6.89E-07	0.005607
GO:0042391	regulation of membrane potential	biological_process	5.46E-07	0.005607
GO:0043085	positive regulation of catalytic activity	biological_process	6.31E-07	0.005607
GO:0043489	RNA stabilization	biological_process	6.35E-07	0.005607
GO:0044089	positive regulation of cellular component biogenesis	biological_process	2.29E-07	0.005607
GO:0044304	main axon	cellular_component	5.88E-07	0.005607
GO:0044708	single-organism behavior	biological_process	5.08E-08	0.002273
GO:0044853	plasma membrane raft	cellular_component	2.54E-07	0.005607
GO:0048167	regulation of synaptic plasticity	biological_process	1.17E-07	0.002273
GO:0048255	mRNA stabilization	biological_process	6.35E-07	0.005607
GO:0050808	synapse organization	biological_process	7.10E-07	0.005607
GO:0051169	nuclear transport	biological_process	5.69E-07	0.005607
GO:0051338	regulation of transferase activity	biological_process	6.22E-07	0.005607
GO:0051656	establishment of organelle localization	biological_process	3.41E-07	0.005607
GO:0060627	regulation of vesicle-mediated transport	biological_process	3.09E-07	0.005607
GO:0070044	synaptobrevin 2-SNAP-25-syntaxin-1a complex	cellular_component	4.75E-07	0.005607
GO:0071702	organic substance transport	biological_process	4.20E-07	0.005607
GO:0072521	purine-containing compound metabolic process	biological_process	6.22E-07	0.005607
GO:0097526	spliceosomal tri-snRNP complex	cellular_component	3.02E-07	0.005607
GO:1901698	response to nitrogen compound	biological_process	4.31E-07	0.005607
GO:1901879	regulation of protein depolymerization	biological_process	4.25E-07	0.005607
GO:1903052	positive regulation of proteolysis involved in cellular protein catabolic process	biological_process	4.86E-07	0.005607

3.3.3 Reduced ORP6 expression is associated with AD.

Dysregulated cholesterol metabolism is an established risk factor for AD[10-12]. We first sought to compare the expression of ORP6 in healthy as compared to AD brains and determine if ORP6 expression is altered in AD. Our analysis of existing publicly available transcriptomic data of ~2100 human brain samples[23] revealed a marked downregulation of ORP6 expression in the parahippocampal gyrus and temporal cortex of AD patients as compared to normal control subjects (**Figure 9a**). ORP6 was also significantly differentially expressed in astrocytes, excitatory and inhibitory neurons in AD patients[24], with the greatest difference in astrocytes (**Figure 9b**). To test whether ORP6 is altered in mice, we quantified ORP6 levels in hippocampi of 11-month-old transgenic APPSwe/PS1dE9 (APP/PS1) that overproduce Aβ and used extensively in the studies of AD pathogenesis[25]. At both the mRNA and protein level, we observed reduced ORP6 expression in the hippocampi (**Figure 9c-e**). We also found that reduced ORP6 expression in hippocampi of AD brains were inversely correlated with hippocampal expression of the LD marker PLIN2 (**Figure 9d** and **9f**).

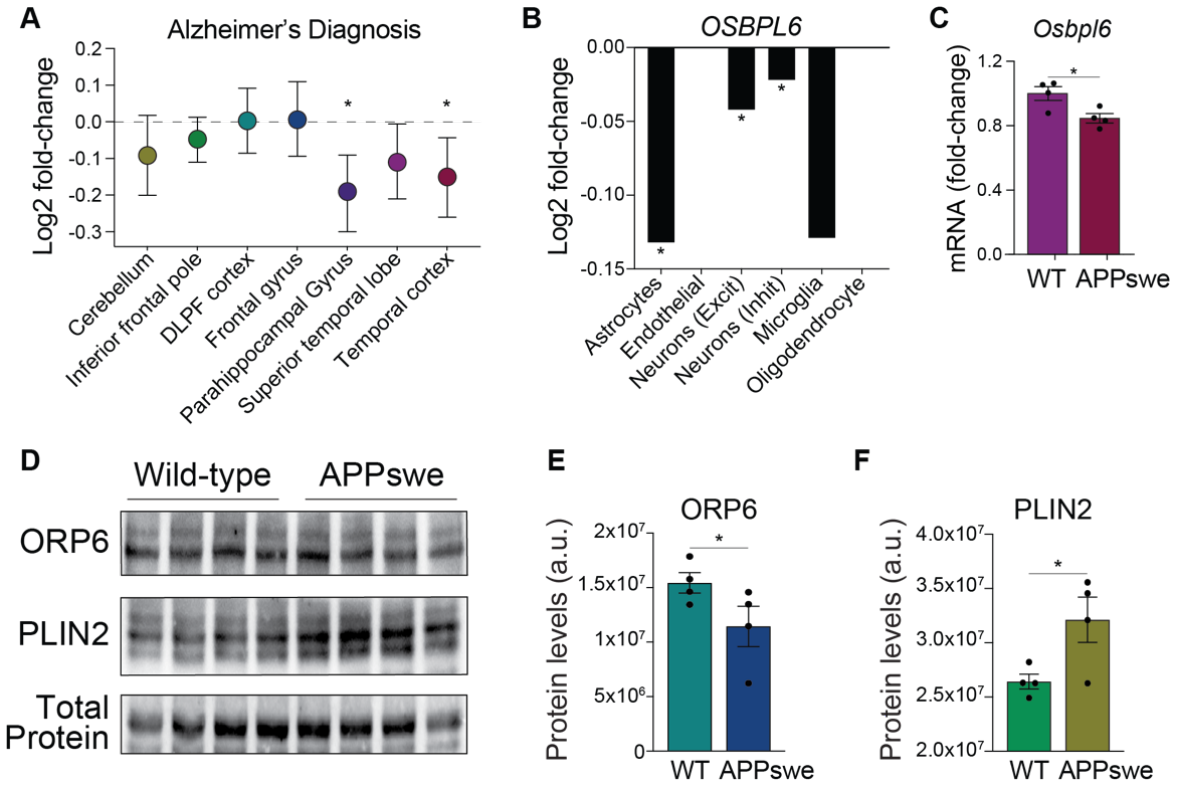

Figure 9. ORP6 expression is altered in AD in mice and humans.

(**A**) Differential expression of ORP6 between AD and control cases across different brain regions using the Annotator for Genes of Organelle from the Reference sequence Analysis (AGORA) web application. Data is expressed as Log2 fold-change ± SEM (**B**) Differential expression of *Osbpl6* in prefrontal cortex of AD and healthy (NC) patients using single-nucleus RNA sequencing (snRNA-Seq). Data extracted from Lau et al.[24] and expressed as Log2 fold change across individual cell type of the brain. (**C**) qRT-PCR quantification of ORP6 mRNA in WT and APPswe mouse hippocampi (n=4 mice/genotype, mean ± SEM). (**D**) Immunoblotting of ORP6 and Plin2 in either wildtype or APPswe mouse brain hippocampus. (**E-F**) Densitometry of ORP6 (E) and Plin2 (F) protein expression normalized to total protein (n=4 mice/genotype, mean ± SEM).

3.3.4 ORP6 ablation in mice causes neuroanatomical changes and impaired neuromuscular function.

Since multiple pathways related to AD were altered in the *Osbpl6*$^{-/-}$ mice, we tested if *Osbpl6*$^{-/-}$ mice exhibit early signs of AD. Meta-analyses of longitudinal cohort studies have identified lower grip strengths as the earliest indicator of cognitive decline, whereby individuals with poorer grip strength have more risk of AD[26,27]. Comparison of forelimb grip strength or forelimb and hindlimb grip strength together in WT and *Osbpl6*$^{-/-}$ mice revealed impaired forelimb and all limb grip strength in female *Osbpl6*$^{-/-}$ mice as compared to WT (**Figure 10a** and **10b**). Moreover, studies have indicated that the hippocampus which is affected in AD, is involved in the regulation of prepulse inhibition (PPI) [119]. As such, we next quantified PPI, which measures sensorimotor gating and the ability of an animal to appropriately process and response to external stimuli. We observed a higher startle response in *Osbpl6*$^{-/-}$ male mice was observed compared to WT (**Figure 10c**).

Altered neuroanatomy as well as reduced neuroanatomical plasticity has been previously described for Aβ models of AD in mice[120]. Using high-resolution post-mortem MRI, we found that overall brain volume was on average 3.2% smaller in *Osbpl6*$^{-/-}$ mice (438.4 mm +/- 14.27 mm^3) as compared to age-matched WT controls (452.8 +/- 11.67 mm^3) (**Figure 10d**). Additionally, we found absolute structure- and voxel-wise differences between the wild-type and homozygote brains in multiple brain regions (**Figure 10e** and **10f**). Volumetric analyses of brain structures revealed that 45 of 182 structures were significantly smaller in *Osbpl6*$^{-/-}$ mice relative to WT (FDR < 0.05) including the thalamus, fornix, corpus callosum and regions of the hippocampus with the most significant differences found in structures such as the hypothalamus, medulla, pons, posterior commissure, and dentate nucleus (FDR < 0.01) as indicated by the blue-turquoise colours in the plots (**Figure 10e**). Collectively, dysregulated brain lipid profiles and increased levels of desmosterol in *Osbpl6*$^{-/-}$ mice as compared to WT combined with neuroanatomical changes and impaired neuromuscular function and increased startle reflex in these mice suggest a protective role for ORP6 against the development of AD.

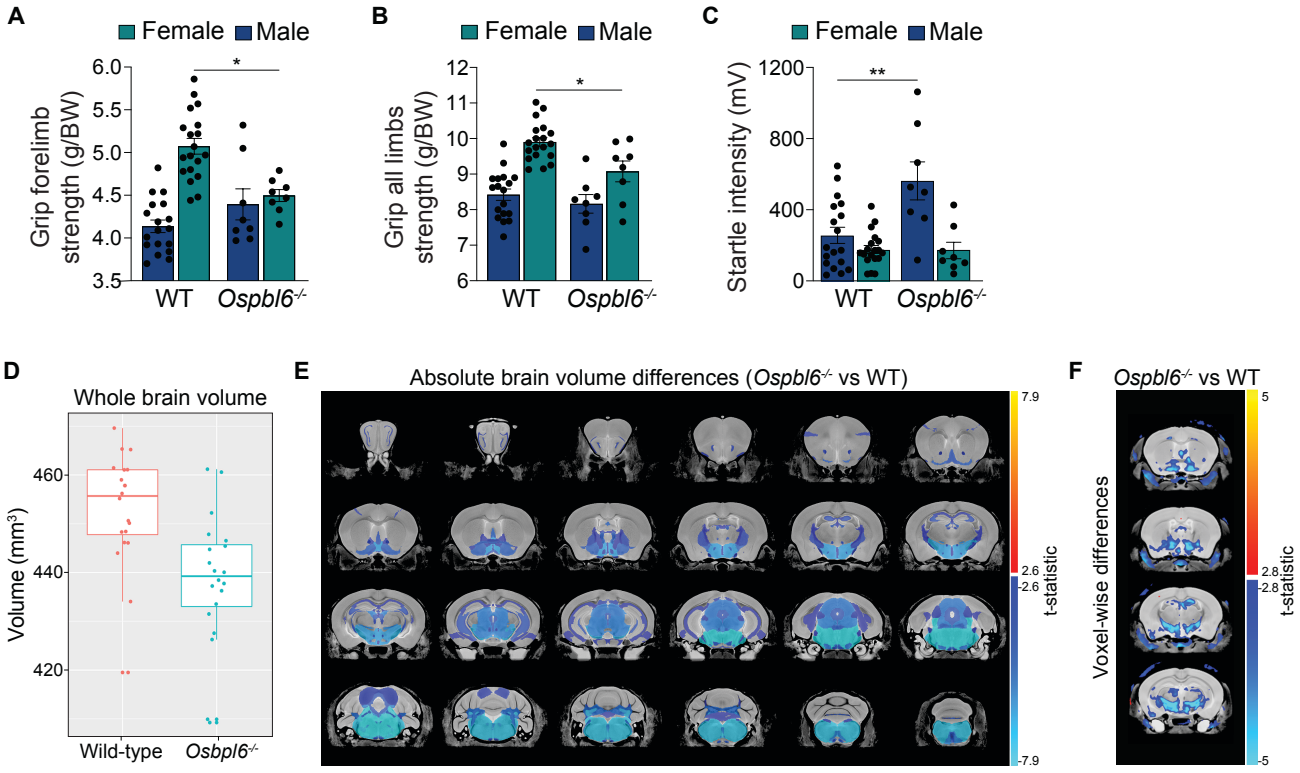

Figure 10. Loss of ORP6 in mice results in brain hypotrophy, impairing neuromuscular function. Grip strength of forelimbs (**A**) or all limbs (**B**) of WT and *Osbpl6*$^{-/-}$ mice at 9 weeks based on the average of 3 independent trials normalized to body weight. (mean± SEM, n=18-19 for WT and n=8 for *Osbpl6*$^{-/-}$). **(C)** Prepulse inhibition startle intensity at 110 dB of WT and *Osbpl6*$^{-/-}$ mice at 9 weeks. (mean ± SEM, n=18-19 for WT and n=8 for *Osbpl6*$^{-/-}$). **(D-F)** Magnetic resonance imaging of WT as compared to *Osbpl6*$^{-/-}$ mouse brains (n=10 WT females, n=10 *Osbpl6*$^{-/-}$ females, n=10 WT males, n=10 *Osbpl6*$^{-/-}$ males). Differences in total brain volume between genotypes are observed in (D), and a significant neuroanatomical effect of *Osbpl6* deletion relative to WT is visualized using *t*-statistics on a structural (E) and voxel-wise (F) level. Regions larger or smaller in *Osbpl6*$^{-/-}$ mutants relative to WT are given red-yellow and blue-turquoise colours, respectively, if effects are significant at an FDR of 5%. #P<0.1, *P<0.05, **P<0.005, ***P<0.0005.

3.3.5 *ORP6 knockdown in mouse astrocytes reduces plasma membrane cholesterol, promotes APP processing and soluble Aβ oligomer production.*

In the CNS, amyloid beta peptides arise from amyloid precursor protein (APP) cleavage by α- or β-secretase enzymes that generate αAPP or βAPP and the shorter α-cleaved COOH-terminal stub of APP subsequently cleaved by γ-secretases[29]. APP, β- and α-secretases all localize to cholesterol-rich membrane domains[29-32]. As such, cholesterol concentrations in membrane microdomains regulate APP processing, and dysregulated cholesterol trafficking in the CNS contributes to AD development[30,33,34]. In light of our previous finding that ORP6 regulates intracellular cholesterol trafficking between cell compartments including the plasma membrane[6], along with increased desmosterol levels observed in mouse brain homogenates of mice lacking ORP6 relative to WT mice (**Figure 7c**) that suggest reduced efficiency of the ultimate step of the cholesterol biosynthesis pathway, we wondered if alterations in astrocyte plasma membrane cholesterol upon loss of ORP6 might in turn regulate APP processing and Aβ production. Indeed, intracellular desmosterol levels were markedly increased in C8-D1A astrocytes upon ORP6 knockdown (**Figure 11a**), suggesting reduced activity of DHCR24 that catalyzes the conversion of desmosterol to cholesterol (**Figure 11b**). DHCR24 expression was reduced at both the mRNA and protein levels in C8-D1A cells treated with ORP6 siRNA as compared to control siRNA-treated cells (**Figure 11c** and **11d**). Plasma membrane cholesterol content was reduced upon ORP6 knockdown in C8-D1A astrocytes concomitant with increased APP processing as observed by reduced intracellular APP and conversely increased extracellular APP (**Figure 11f**), resulting in increased extracellular but not intracellular soluble Aβ oligomers (**Figure 11g** and **11h**). Taken together, this data demonstrates that ORP6 regulates plasma membrane cholesterol content, APP processing and soluble Aβ oligomer production in mouse astrocytes and this could be due to decrease in DHCR24 leading to increased desmosterol (**Figure 12**).

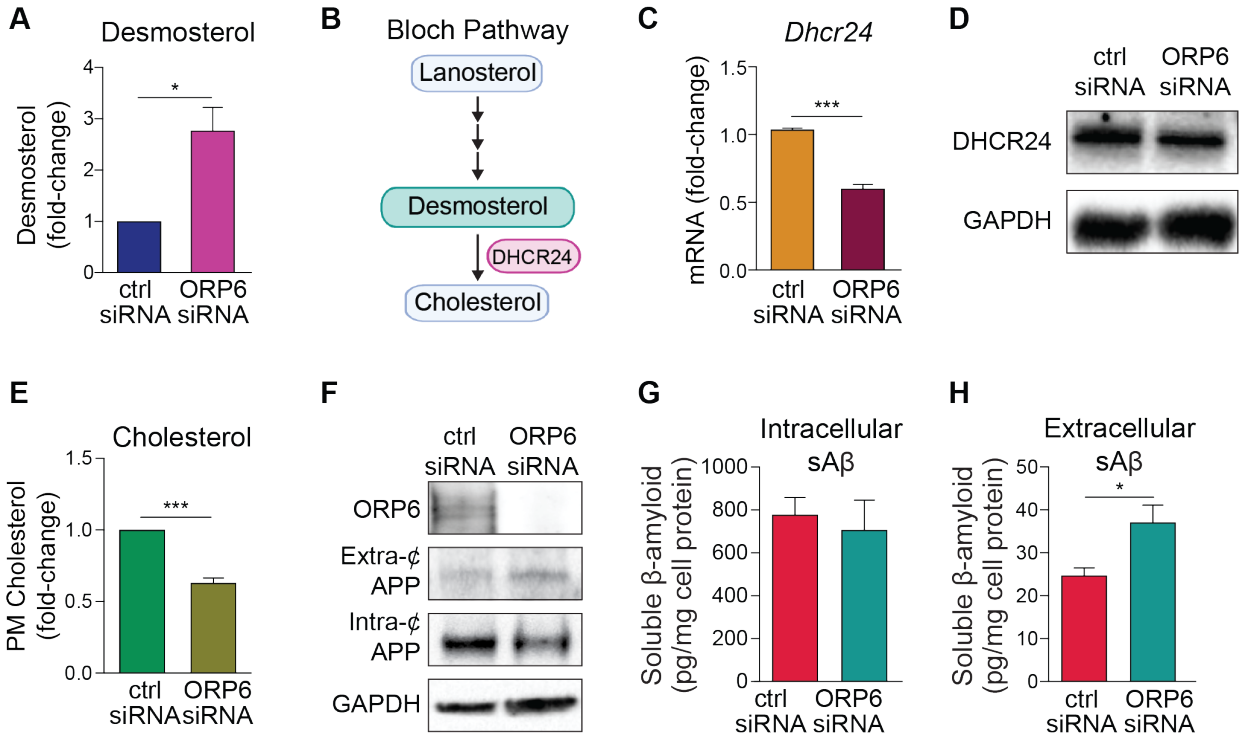

Figure 11. ORP6 knockdown promotes astrocytic amyloid-beta production by reducing plasma membrane cholesterol content and increasing APP trafficking and processing.

(**A**) Relative intracellular desmosterol content as quantified by thin layer chromatography of C8-D1A cells transfected with ctrl or ORP6 siRNA and loaded with ^{3}H-mevalonate for 24hr (n=3). (**B**) Schematic overview of the cholesterol biosynthesis pathway preferentially used in astrocytes, the Bloch Pathway, where desmosterol is the immediate precursor to cholesterol and this ultimate step in *de novo* cholesterol synthesis is catalyzed by DHCR24. (**C**) qRT-PCR of *Dhcr24* mRNA in ORP6 as compared to ctrl siRNA-treated C8-D1A cells (n=3, mean ± SEM). (**D**) Immunoblotting of DHCR24 and GAPDH in C8-D1A cells transfected with ctrl or ORP6 siRNA. Image is representative of n=5 independent experiments. (**E**) Quantification of *de novo* synthesized plasma membrane (PM) ^{3}H-cholesterol content extracted from cells radiolabelled as in (A). Cholesterol was extracted from the PM by incubation of cells with 10mM mβ-CD at 4˚C for 15 mins (n=3, mean ± SEM). (**F**) Immunoblotting of ORP6, extra- or intra-cellular (extra-¢ or intra-¢) amyloid precursor protein (APP) and GAPDH in C8-D1A cells transfected with ctrl or ORP6 siRNA. Image is representative of n=5 independent experiments. (**G**) Intracellular or (**H**) extracellular Aβ oligomer concentrations (pg/mg protein) in cells treated as in (F) (n=3, mean ± SEM). *P<0.05, **P<0.005, ***P<0.0005 by Student's t-test (A, C, E, G, H).

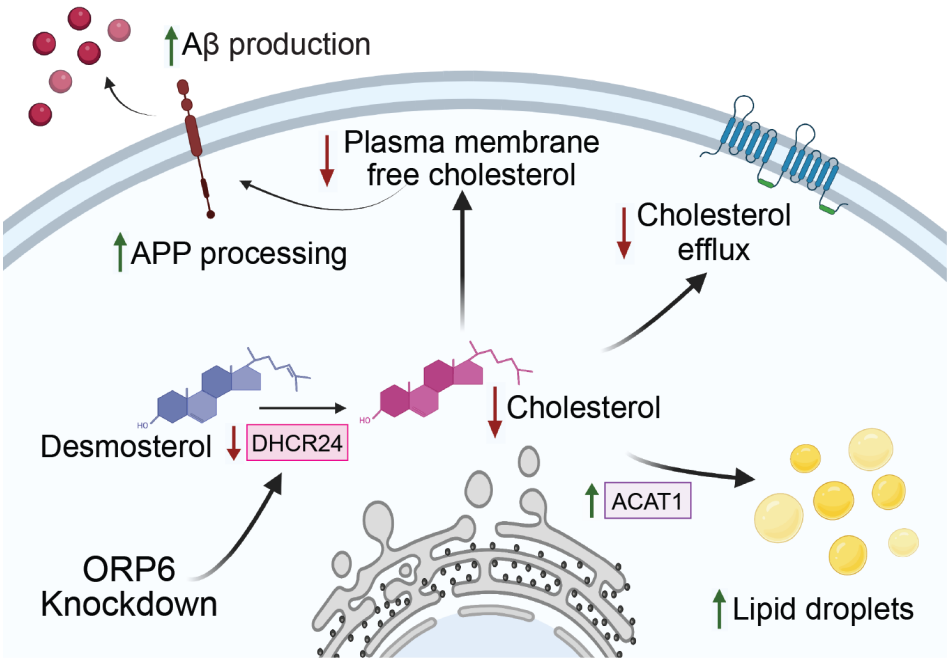

Figure 12. Schematic overview of the proposed mechanism by which ORP6 promotes astrocytic Aβ production.

APP: amyloid precursor protein; Aβ: amyloid beta; ACAT1: Acyl-coenzyme A: cholesterol acyltransferase; DHCR24: 24-Dehydrocholesterol reductase; ORP6: oxysterol-binding protein-related protein 6. Created with BioRender.com

4. DISCUSSION

4.1 General discussion

While cholesterol homeostasis is a fundamental and highly regulated process, our understanding of cholesterol trafficking between cell compartments remains incomplete. Fluctuations in cellular cholesterol concentrations are sensed by SREBPs and the sterol responsive LXRs that coordinate the expression of cholesterol biosynthesis, uptake and efflux genes. These intricate cholesterol-sensing pathways entail coordinated inter-membrane cholesterol transport, facilitated by lipid transfer proteins. To date, several lipid transfer proteins exhibit the capacity for mediating sterol transfer *in vitro,* yet assigning physiologic roles for these remains challenging. Only a handful of intracellular cholesterol-transfer proteins were attributed clear physiologic functions *in vivo*: Niemann Pick Type C proteins 1 and 2 (NPC1, NPC2) that are required for lysosome cholesterol export[35], steroid acute regulatory protein (STARD1) that is required for cholesterol traffic to the inner mitochondrial membrane[36,37], and more recently Aster proteins that shuttle cholesterol between ER-plasma membrane contact sites[38]. Here, we identify LXR-regulated ORP6, one of the least studied members of the ORP family of lipid transfer proteins, as a regulator of cholesterol homeostasis in astrocytes and the CNS.

4.2 ORP6 in glial cholesterol homeostasis

In this thesis, we present ORP6 as a regulator of cholesterol homeostasis in astrocytes, the major cholesterol producers of the brain. While it was previously shown that ORP6 regulates macrophage and hepatic cholesterol homeostasis, here we report that ORP6 expression is significantly enriched in the brain relative to any other tissue, specifically in astrocytes and within the hippocampus brain region. Among the different cell types of the brain, astrocytes serve the most diverse roles, most notably providing structural and functional support for neurons[121]. We demonstrate that ORP6 knockdown reduced astrocytic cholesterol efflux to lipid-poor apoA-I and HDL, while increasing cellular cholesterol esterification within LDs. Second to astrocytes, we found that ORP6 was also highly expressed in neurons. While the role of ORP6 in neurons was not investigated in this study, ORP6 was previously found to localize to ER-PM contact sites in cerebellar neurons and to regulate the turnover of phophtidylinositol-4-phosphate, implicating

ORP6 in neuronal pathology[65]. These results have broader implications in overall brain functions as impaired cholesterol metabolism in glial cells could underlie neurological diseases[65] by regulating synaptic transmission in neurons via lipid metabolism[122]. Astrocyte-derived cholesterol is utilized by neurons to modulate lipid raft formation and membrane fluidity, subsequently regulating neurotransmission and localization of proteins such as APP on neuronal membranes [89,122]. Furthermore, astrocytes can form LDs in response to neuronal stress when overstimulated neurons shuttle their peroxidised fatty acids (FAs) to astrocytes[123]. As such, altered astrocytic cholesterol homeostasis may impact neuronal function and health. Thus, understanding the implication of cholesterol trafficking in the astrocyte-neuron crosstalk is important. While in this study the role of ORP6 was only investigated in astrocytes, future work is needed to address the role of glial ORP6 in crosstalk between astrocytes and neurons, as well as the role of ORP6 in neuronal function.

4.3 Whole body effect of ORP6

Most of our knowledge on the structural and functional roles of ORPs thus far stems from studies of the *Saccharomyces cerevisiae* OSBP homologues (Osh) proteins, Osh1p-Osh7p[39]. Intriguingly, the collective mutation of all Osh proteins and even ORB proteins are embryonic lethal[51,52] . Understanding the physiological role of ORPs in mice has proven difficult due to a lack of available genetic mouse models. In the past, deleting OSBP in mice was unsuccessful as it caused early embryonic death[53]. In 2013, the first viable ORP knockout mouse model successfully developed[54]. We herein present a newly generated second viable ORP6 family member knockout mouse.

ORP6-deficient mice display alterations in whole-body lipid homeostasis, whereby several lipids are altered in *Osbpl6*$^{-/-}$ mice compared to their WT counterpart. Plasma triglyceride levels are unaltered, while total cholesterol and HDL-cholesterol levels are significantly reduced in male *Osbpl6*$^{-/-}$ mice but not females, suggesting a sex-specific function of ORP6 in circulating lipid levels. Similarly, ORP8-deficient mice displayed gender-specific changes in cholesterol biosynthesis intermediates and hepatic gene expression. While no additional ORP knockout mouse model exists, these data suggest that ORPs exhibit some gender-specific functions in lipid

homeostasis and underscore the crucial importance of investigating the two genders separately. Further research gender-specific roles for ORP6 in regulating circulating lipids is warranted to make any other further conclusions.

In the brain, we observed a significant increase in desmosterol concentrations. However, surprisingly the level of cholesterol, the final product of the cholesterol biosynthesis pathway downstream of desmosterol, remains unchanged. This observation could be attributed to the fact that we performed lipidomics on whole brain homogenates and accordingly minute changes in specific regions of the brain were not detectable. Future experiments will be designed to perform cell type- and brain region-specific lipidomic profiling. As our study points to a role for ORP6 in AD pathology, it would be of interest to quantify lipidomic changes in regions altered in AD such as the cortex and hippocampus.

4.4 ORP6 in AD pathogenesis

A SNP in ORP6 was previously identified to have genome-wide significance for the association of AD[67]; however, the expression of ORP6 in AD and its particular role in the pathogenesis of AD remained unexplored. In this study, we provide evidence to support a novel for ORP6 in the pathogenesis of AD. Notably, our results suggest that ORP6 downregulation promotes Aβ production both *in vitro* and *in vivo,* identifying ORP6 as a novel potential therapeutic target for the treatment of AD.

Immunofluorescent staining for ORP6 in mouse brain cross-sections revealed ORP6 to be enriched in the hippocampus, the center of emotion and memory. Furthermore, analysis of existing human databases reveals downregulation of ORP6 expression in the parahippocampal gyrus and temporal cortex of AD patients as compared to normal control subjects. The hippocampus is the brain region most vulnerable to damage at early stages of AD. Moreover, ORP6 expression was strikingly reduced in astrocytes from AD patients as compared to normal control subjects[23]. In mice, we observed reduced ORP6 expression at both the mRNA and protein levels in the hippocampus of AD mice. The mechanisms by which ORP6 expression is dysregulated in AD in both mice and humans is unknown. Recent evidence reveals that miR-33, a potent post-translational regulator of lipid metabolism, is highly expressed in the brain where it can drive AD

by promoting Aβ secretion and impairing Aβ clearance[124]. Conversely, miR-33 knockdown was shown to protect against Aβ (25-35)-induced inflammation, oxidative stress, apoptosis, and synaptic damage[125]. Given that 1. increased SREBP-2 nuclear activity in the CNS contributes to AD pathogenesis[85], 2. active SREBP-2 upregulates its own transcription in a feed-forward positive regulatory loop, 3. miR-33 is co-transcribed with SREBP-2 and 4. ORP6 is a major gene target of miR-33[62], reduced ORP6 expression in AD might be attributable to elevated SREBP-2/miR-33 expression.

Remarkably, in our study ORP6 deletion in young mice (4 months-old) alone with no aging or dietary intervention was sufficient to drive a significant accumulation of neurotoxic oligomeric Aβ, produce neuroanatomical changes and impair neuromuscular function. Mounting evidence suggests that accumulation of soluble Aβ, even in the absence of Aβ plaques, can singularly drive the development of AD-related learning and memory deficits[126]. In line with this, *Osbpl6*$^{-/-}$ mice exhibited early signs of AD, such as lower grip strengths[127,128] and excessive excitatory glutamatergic neurotransmission that consist of the earliest indicators of cognitive decline underlying neurodegeneration in AD[129,130]. Moreover, ORP6 deficient mice exhibited dysregulation of whole-body lipid homeostasis, some of which are characteristic of AD[131,132], including downregulation of LPC in the plasma of *Osbpl6*$^{-/-}$ mice relative to WT.

Aβ plays a central role in AD pathogenesis and, while neurons are major sources of Aβ in the brain, astrocytes outnumber neurons by more than 5-fold[133]. Mounting evidence suggests that even minute quantities of astrocytic Aβ production could significantly contribute to Aβ in AD[133,134]. Here, we demonstrate a direct role for ORP6 as regulator of amyloidogenic APP processing in astrocytes. We show that ORP6 downregulates DHCR24, resulting in accumulation of desmosterol and reduced plasma membrane cholesterol content. In line with previous reports of disorganized lipid rafts and an inverse relationship between DHCR24 expression and APP-mediated Aβ production[135], we show that downregulation of DHCR24 and plasma membrane cholesterol in ORP6 knock down astrocytes increases APP processing and Aβ production (**Figure 12**).

4.5 HDL metabolism and AD

In the peripheral nervous system (PNS), emerging evidence points to circulating HDL plasma levels as a new biomarker for AD [72,75–77]. Here, treatment with ORP6 siRNA in astrocytes reduced the expression of HDL metabolism genes, including *Apod*, *Apof*, and *Apol8* apolipoproteins and the cholesterol transporter *Abcg1*, while loss of ORP6 function in mice resulted in a marked reduction in plasma HDL. Our observations are consistent with the fact that 1. the *OSBPL6* gene resides in a locus on chromosome 2 linked to premature coronary artery disease[60] and variations in HDL-cholesterol levels[136], 2. ORP6 mediates cholesterol traffic between intracellular compartments and the plasma membrane for efflux[61] and 3. hepatic levels of *OSBPL6* mRNA are positively correlated with plasma levels of HDL-cholesterol and apoA1 in humans[61]. Notably, several other ORP members were also reported to alter circulating lipoproteins concentrations. ORP8 regulates HDL-cholesterol, while ORP10 knockdown in human hepatocytes promotes apolipoprotein B-100 secretion, triglyceride synthesis and secretion[137]. Finally, a SNP in ORP7 showed genome-wide significant association with serum LDL-cholesterol and total cholesterol concentrations[138], several SNPs in the *OSBPL11* gene are associated with cardiovascular disease risk factors including LDL-cholesterol plasma levels and hyperglycemia[139], and polymorphisms in the *OSBPL10* gene are associated with dyslipidemias and peripheral artery disease[140–142].

Mechanisms underlying the association between plasma HDL and AD are not well understood. Evidence from clinical and preclinical studies as well as from bioengineered arteries supports the hypothesis that HDL protects against cerebrovascular dysfunction in AD[79]. Plasma HDL levels inversely correlate with AD, and circulating HDL protects against memory deficits and neuroinflammation and reduces vascular Aβ accumulation[143]. Plasma lipoproteins cannot enter the brain owing to the impermeable blood-brain barrier. However, the movement of lipoprotein particles across this barrier is not completely impossible, whereby studies show that HDL particles can enter the brain through transcytosis or selective uptake[144–146]. This suggests that systemic changes in plasma HDL-cholesterol levels induced by ORP6 deficiency in mice could drive alterations in brain lipid metabolism observed in *Osbpl6*$^{-/-}$ mice relative to WT.

5. CONCLUSION

In summary, we highlight a critical role for cholesterol trafficking proteins in brain cholesterol homeostasis and function. We show that ORP6 is highly expressed in the brain within astrocytes and neurons. PCR array profiling revealed altered expression of cholesterol biosynthesis and efflux genes upon ORP6 inhibition in astrocytes. Consistent with this, we observed reduced cholesterol efflux, increased desmosterol, and cytosolic LD accumulation in astrocytes upon ORP6 silencing, highlighting a role for ORP6 in astrocyte cholesterol homeostasis. We also present a newly generated second viable ORP family member knockout mouse and identify ORP6 as a critical regulator of brain and whole-body lipid homeostasis. We show that ORP6-deficient mice display dysregulated plasma and brain lipid profiles and are susceptible to neuroanatomical alterations and increased production of soluble Aβ, pointing to a role for ORP6 in AD pathogenesis. We propose that ORP6 regulates Aβ production and the development of AD by regulating the conversion of desmosterol to cholesterol and thus the levels of membrane cholesterol and APP-dependent Aβ production. Future studies will investigate the long-term effects of ORP6 deficiency in the context of AD, such as the development of cognitive impairments and amyloid plaques. This thesis expands our understanding of brain lipid homeostasis and provides a novel mechanism for AD.

REFERENCES

1. Luo, J., Yang, H. & Song, B.-L. Mechanisms and regulation of cholesterol homeostasis. *Nat. Rev. Mol. Cell Biol.* **21**, 225–245 (2020).
2. Berg JM, Tymoczko JL, S. L. Important Derivatives of Cholesterol Include Bile Salts and Steroid Hormones. in *Biochemistry* (W H Freeman, 2002).
3. Chang, T.-Y., Yamauchi, Y., Hasan, M. T. & Chang, C. Cellular cholesterol homeostasis and Alzheimer's disease. *J. Lipid Res.* **58**, 2239–2254 (2017).
4. Orth, M. & Bellosta, S. Cholesterol: Its regulation and role in central nervous system disorders. *Cholesterol* **2012**, 292598 (2012).
5. Pfrieger, F. W. Role of cholesterol in synapse formation and function. *Biochim. Biophys. Acta* **1610**, 271–280 (2003).
6. Zhang, J. & Liu, Q. Cholesterol metabolism and homeostasis in the brain. *Protein Cell* **6**, 254–264 (2015).
7. Ferris, H. A. *et al.* Loss of astrocyte cholesterol synthesis disrupts neuronal function and alters whole-body metabolism. *Proc. Natl. Acad. Sci. U. S. A.* **114**, 1189–1194 (2017).
8. Hussain, G. *et al.* Role of cholesterol and sphingolipids in brain development and neurological diseases. *Lipids Health Dis.* **18**, 26 (2019).
9. Arenas, F., Garcia-Ruiz, C. & Fernandez-Checa, J. C. Intracellular Cholesterol Trafficking and Impact in Neurodegeneration. *Front. Mol. Neurosci.* **10**, 382 (2017).
10. Dai, L. *et al.* Cholesterol Metabolism in Neurodegenerative Diseases: Molecular Mechanisms and Therapeutic Targets. *Mol. Neurobiol.* **58**, 2183–2201 (2021).
11. Skubic, C. & Rozman, D. Sterols from the Post-Lanosterol Part of Cholesterol Synthesis: Novel Signaling Players BT - Mammalian Sterols : Novel Biological Roles of Cholesterol Synthesis Intermediates, Oxysterols and Bile Acids. in (eds. Rozman, D. & Gebhardt, R.) 1–22 (Springer International Publishing, 2020). doi:10.1007/978-3-030-39684-8_1
12. Genaro-Mattos, T. C., Anderson, A., Allen, L. B., Korade, Z. & Mirnics, K. Cholesterol Biosynthesis and Uptake in Developing Neurons. *ACS Chem. Neurosci.* **10**, 3671–3681 (2019).
13. Petrov, A. M., Kasimov, M. R. & Zefirov, A. L. Brain Cholesterol Metabolism and Its

Defects: Linkage to Neurodegenerative Diseases and Synaptic Dysfunction. *Acta Naturae* **8**, 58–73 (2016).

14. Orth, M. & Bellosta, S. Cholesterol: Its regulation and role in central nervous system disorders. *Cholesterol* **2012**, (2012).
15. Pfrieger, F. W. Cholesterol homeostasis and function in neurons of the central nervous system. *Cell. Mol. Life Sci.* **60**, 1158–1171 (2003).
16. Berghoff, S. A. *et al.* Microglia facilitate repair of demyelinated lesions via post-squalene sterol synthesis. *Nat. Neurosci.* **24**, 47–60 (2021).
17. van Deijk, A.-L. F. *et al.* Astrocyte lipid metabolism is critical for synapse development and function in vivo. *Glia* **65**, 670–682 (2017).
18. Bohlen, C. J. *et al.* Diverse Requirements for Microglial Survival, Specification, and Function Revealed by Defined-Medium Cultures. *Neuron* **94**, 759-773.e8 (2017).
19. Litvinov, D. Y., Savushkin, E. V & Dergunov, A. D. Intracellular and Plasma Membrane Events in Cholesterol Transport and Homeostasis. *J. Lipids* **2018**, 3965054 (2018).
20. Maxfield, F. R. & Tabas, I. Role of cholesterol and lipid organization in disease. *Nature* **438**, 612–621 (2005).
21. Liu, K. & Czaja, M. J. Regulation of lipid stores and metabolism by lipophagy. *Cell Death Differ.* **20**, 3–11 (2013).
22. Mahley, R. W. Central Nervous System Lipoproteins: ApoE and Regulation of Cholesterol Metabolism. *Arterioscler. Thromb. Vasc. Biol.* **36**, 1305–1315 (2016).
23. Courtney, R. & Landreth, G. E. LXR Regulation of Brain Cholesterol: From Development to Disease. *Trends Endocrinol. Metab.* **27**, 404–414 (2016).
24. Dietschy, J. M. Central nervous system: cholesterol turnover, brain development and neurodegeneration. *Biol. Chem.* **390**, 287–293 (2009).
25. Chen, J., Zhang, X., Kusumo, H., Costa, L. G. & Guizzetti, M. Cholesterol efflux is differentially regulated in neurons and astrocytes: implications for brain cholesterol homeostasis. *Biochim. Biophys. Acta* **1831**, 263–275 (2013).
26. Eberlé, D., Hegarty, B., Bossard, P., Ferré, P. & Foufelle, F. SREBP transcription factors: Master regulators of lipid homeostasis. *Biochimie* **86**, 839–848 (2004).

27. Soccio, R. E. & Breslow, J. L. Intracellular cholesterol transport. *Arterioscler. Thromb. Vasc. Biol.* **24**, 1150–1160 (2004).
28. Fernández-Hernando, C. & Moore, K. J. MicroRNA modulation of cholesterol homeostasis. *Arterioscler. Thromb. Vasc. Biol.* **31**, 2378–2382 (2011).
29. Vaya, J. & Schipper, H. M. Oxysterols, cholesterol homeostasis, and Alzheimer disease. *J. Neurochem.* **102**, 1727–1737 (2007).
30. Björkhem, I. & Diczfalusy, U. Side-Chain Oxidized Oxysterols in Health and Disease BT - Mammalian Sterols : Novel Biological Roles of Cholesterol Synthesis Intermediates, Oxysterols and Bile Acids. in (eds. Rozman, D. & Gebhardt, R.) 41–79 (Springer International Publishing, 2020). doi:10.1007/978-3-030-39684-8_3
31. Gamba, P. *et al.* The Controversial Role of 24-S-Hydroxycholesterol in Alzheimer's Disease. *Antioxidants (Basel, Switzerland)* **10**, (2021).
32. Lev, S. Non-vesicular lipid transport by lipid-transfer proteins and beyond. *Nat. Rev. Mol. Cell Biol.* **11**, 739–750 (2010).
33. Voelker, D. R. Organelle biogenesis and intracellular lipid transport in eukaryotes. *Microbiol. Rev.* **55**, 543–560 (1991).
34. Maxfield, F. R. & Wüstner, D. Intracellular cholesterol transport. *J. Clin. Invest.* **110**, 891–898 (2002).
35. Prinz, W. A. Non-vesicular sterol transport in cells. *Prog. Lipid Res.* **46**, 297–314 (2007).
36. Scorrano, L. *et al.* Coming together to define membrane contact sites. *Nat. Commun.* **10**, 1287 (2019).
37. Jain, A. & Holthuis, J. C. M. Membrane contact sites, ancient and central hubs of cellular lipid logistics. *Biochim. Biophys. acta. Mol. cell Res.* **1864**, 1450–1458 (2017).
38. Lehto, M. *et al.* The OSBP-related protein family in humans. *J. Lipid Res.* **42**, 1203–1213 (2001).
39. Kentala, H., Weber-Boyvat, M. & Olkkonen, V. M. OSBP-Related Protein Family: Mediators of Lipid Transport and Signaling at Membrane Contact Sites. *Int. Rev. Cell Mol. Biol.* **321**, 299–340 (2016).
40. Wong, L. H., Gatta, A. T. & Levine, T. P. Lipid transfer proteins: the lipid commute via

shuttles, bridges and tubes. *Nat. Rev. Mol. Cell Biol.* **20**, 85–101 (2019).

41. Wilhelm, L. P. *et al.* STARD3 mediates endoplasmic reticulum-to-endosome cholesterol transport at membrane contact sites. *EMBO J.* **36**, 1412–1433 (2017).
42. Larsen, M. C., Lee, J., Jorgensen, J. S. & Jefcoate, C. R. STARD1 Functions in Mitochondrial Cholesterol Metabolism and Nascent HDL Formation. Gene Expression and Molecular mRNA Imaging Show Novel Splicing and a 1:1 Mitochondrial Association. *Front. Endocrinol. (Lausanne).* **11**, 559674 (2020).
43. Peake, K. B. & Vance, J. E. Defective cholesterol trafficking in Niemann-Pick C-deficient cells. *FEBS Lett.* **584**, 2731–2739 (2010).
44. Torres, S., García-Ruiz, C. M. & Fernandez-Checa, J. C. Mitochondrial Cholesterol in Alzheimer's Disease and Niemann-Pick Type C Disease. *Front. Neurol.* **10**, 1168 (2019).
45. Sandhu, J. *et al.* Aster Proteins Facilitate Nonvesicular Plasma Membrane to ER Cholesterol Transport in Mammalian Cells. *Cell* **175**, 514-529.e20 (2018).
46. Vihervaara, T. *et al.* Cytoplasmic oxysterol-binding proteins: sterol sensors or transporters? *Chem. Phys. Lipids* **164**, 443–450 (2011).
47. Fairn, G. D. & McMaster, C. R. Emerging roles of the oxysterol-binding protein family in metabolism, transport, and signaling. *Cell. Mol. Life Sci.* **65**, 228–236 (2008).
48. Tong, J., Yang, H., Yang, H., Eom, S. H. & Im, Y. J. Structure of Osh3 reveals a conserved mode of phosphoinositide binding in oxysterol-binding proteins. *Structure* **21**, 1203–1213 (2013).
49. Raychaudhuri, S. & Prinz, W. A. The diverse functions of oxysterol-binding proteins. *Annu. Rev. Cell Dev. Biol.* **26**, 157–177 (2010).
50. Olkkonen, V. M. & Li, S. Oxysterol-binding proteins: sterol and phosphoinositide sensors coordinating transport, signaling and metabolism. *Prog. Lipid Res.* **52**, 529–538 (2013).
51. Beh, C. T., Cool, L., Phillips, J. & Rine, J. Overlapping functions of the yeast oxysterol-binding protein homologues. *Genetics* **157**, 1117–1140 (2001).
52. Kobuna, H. *et al.* Multivesicular body formation requires OSBP-related proteins and cholesterol. *PLoS Genet.* **6**, (2010).
53. Antonny, B., Bigay, J. & Mesmin, B. The Oxysterol-Binding Protein Cycle: Burning Off

PI(4)P to Transport Cholesterol. *Annu. Rev. Biochem.* **87**, 809–837 (2018).

54. Béaslas, O. *et al.* Osbpl8 deficiency in mouse causes an elevation of high-density lipoproteins and gender-specific alterations of lipid metabolism. *PLoS One* **8**, e58856 (2013).
55. Pietrangelo, A. & Ridgway, N. D. Bridging the molecular and biological functions of the oxysterol-binding protein family. *Cell. Mol. Life Sci.* **75**, 3079–3098 (2018).
56. Taylor, F. R. & Kandutsch, A. A. Oxysterol binding protein. *Chem. Phys. Lipids* **38**, 187–194 (1985).
57. Mesmin, B. *et al.* A four-step cycle driven by PI(4)P hydrolysis directs sterol/PI(4)P exchange by the ER-Golgi tether OSBP. *Cell* **155**, 830–843 (2013).
58. Chung, J. *et al.* INTRACELLULAR TRANSPORT. PI4P/phosphatidylserine countertransport at ORP5- and ORP8-mediated ER-plasma membrane contacts. *Science* **349**, 428–432 (2015).
59. Olkkonen, V. M. & Ikonen, E. Cholesterol transport in the late endocytic pathway: Roles of ORP family proteins. *J. Steroid Biochem. Mol. Biol.* **216**, 106040 (2022).
60. Nsengimana, J. *et al.* Enhanced linkage of a locus on chromosome 2 to premature coronary artery disease in the absence of hypercholesterolemia. *Eur. J. Hum. Genet.* **15**, 313–319 (2007).
61. Ouimet, M. *et al.* miRNA Targeting of Oxysterol-Binding Protein-Like 6 Regulates Cholesterol Trafficking and Efflux. *Arterioscler. Thromb. Vasc. Biol.* **36**, 942–951 (2016).
62. Mireille, O. *et al.* miRNA Targeting of Oxysterol-Binding Protein-Like 6 Regulates Cholesterol Trafficking and Efflux. *Arterioscler. Thromb. Vasc. Biol.* **36**, 942–951 (2016).
63. Lehto, M., Tienari, J., Lehtonen, S., Lehtonen, E. & Olkkonen, V. M. Subfamily III of mammalian oxysterol-binding protein (OSBP) homologues: the expression and intracellular localization of ORP3, ORP6, and ORP7. *Cell Tissue Res.* **315**, 39–57 (2004).
64. Brain RNA-Seq. (2014). Available at: http://www.brainrnaseq.org/. (Accessed: 29th November 2019)
65. Mochizuki, S. *et al.* Oxysterol-binding protein-related protein (ORP) 6 localizes to the ER and ER-plasma membrane contact sites and is involved in the turnover of PI4P in

cerebellar granule neurons. *Exp. Cell Res.* **370**, 601–612 (2018).

66. Mochizuki, S., Miki, H., Zhou, R. & Noda, Y. The involvement of oxysterol-binding protein related protein (ORP) 6 in the counter-transport of phosphatidylinositol-4-phosphate (PI4P) and phosphatidylserine (PS) in neurons. *Biochem. Biophys. reports* **30**, 101257 (2022).
67. Herold, C. *et al.* Family-based association analyses of imputed genotypes reveal genome-wide significant association of Alzheimer's disease with OSBPL6, PTPRG, and PDCL3. *Mol. Psychiatry* **21**, 1608–1612 (2016).
68. Serý, O., Povová, J., Míšek, I., Pešák, L. & Janout, V. Molecular mechanisms of neuropathological changes in Alzheimer's disease: a review. *Folia Neuropathol.* **51**, 1–9 (2013).
69. Gatz, M. *et al.* Role of genes and environments for explaining Alzheimer disease. *Arch. Gen. Psychiatry* **63**, 168–174 (2006).
70. Wollmer, M. A. Cholesterol-related genes in Alzheimer's disease. *Biochim. Biophys. Acta* **1801**, 762–773 (2010).
71. Liu, C.-C., Liu, C.-C., Kanekiyo, T., Xu, H. & Bu, G. Apolipoprotein E and Alzheimer disease: risk, mechanisms and therapy. *Nature reviews. Neurology* **9**, 106–118 (2013).
72. Marsillach, J. *et al.* HDL Proteome and Alzheimer's Disease: Evidence of a Link. *Antioxidants (Basel, Switzerland)* **9**, (2020).
73. Carter, C. J. Convergence of genes implicated in Alzheimer's disease on the cerebral cholesterol shuttle: APP, cholesterol, lipoproteins, and atherosclerosis. *Neurochem. Int.* **50**, 12–38 (2007).
74. Gliozzi, M. *et al.* Cholesterol homeostasis: Researching a dialogue between the brain and peripheral tissues. *Pharmacol. Res.* **163**, 105215 (2021).
75. Iqbal, G., Braidy, N. & Ahmed, T. Blood-Based Biomarkers for Predictive Diagnosis of Cognitive Impairment in a Pakistani Population. *Front. Aging Neurosci.* **12**, 223 (2020).
76. Zhang, X. *et al.* Early-mid adulthood measures of HDL, triglycerides and fasting glucose are associated with late-onset Alzheimer disease. *Alzheimer's Dement.* **16**, e046125 (2020).

77. Merched, A., Xia, Y., Visvikis, S., Serot, J. M. & Siest, G. Decreased high-density lipoprotein cholesterol and serum apolipoprotein AI concentrations are highly correlated with the severity of Alzheimer's disease. *Neurobiol. Aging* **21**, 27–30 (2000).

78. Martinez, A. E. *et al.* The small HDL particle hypothesis of Alzheimer's disease. *Alzheimers. Dement.* (2022). doi:10.1002/alz.12649

79. Button, E. B. *et al.* HDL from an Alzheimer's disease perspective. *Curr. Opin. Lipidol.* **30**, 224–234 (2019).

80. Takahashi, R. H., Nagao, T. & Gouras, G. K. Plaque formation and the intraneuronal accumulation of β-amyloid in Alzheimer's disease. *Pathol. Int.* **67**, 185–193 (2017).

81. Wang, H. *et al.* Regulation of beta-amyloid production in neurons by astrocyte-derived cholesterol. *Proc. Natl. Acad. Sci. U. S. A.* **118**, (2021).

82. Shibuya, Y., Chang, C. C. & Chang, T.-Y. ACAT1/SOAT1 as a therapeutic target for Alzheimer's disease. *Future Med. Chem.* **7**, 2451–2467 (2015).

83. Bryleva, E. Y. *et al.* ACAT1 gene ablation increases 24(S)-hydroxycholesterol content in the brain and ameliorates amyloid pathology in mice with AD. *Proc. Natl. Acad. Sci. U. S. A.* **107**, 3081–3086 (2010).

84. Barbero-Camps, E., Fernández, A., Martínez, L., Fernández-Checa, J. C. & Colell, A. APP/PS1 mice overexpressing SREBP-2 exhibit combined Aβ accumulation and tau pathology underlying Alzheimer's disease. *Hum. Mol. Genet.* **22**, 3460–3476 (2013).

85. Mastrocola, R. *et al.* Dysregulation of SREBP2 induces BACE1 expression. *Neurobiol. Dis.* **44**, 116–124 (2011).

86. Maulik, M., Westaway, D., Jhamandas, J. H. & Kar, S. Role of cholesterol in APP metabolism and its significance in Alzheimer's disease pathogenesis. *Mol. Neurobiol.* **47**, 37–63 (2013).

87. Blanchette-Mackie, E. J. Intracellular cholesterol trafficking: role of the NPC1 protein. *Biochim. Biophys. Acta* **1486**, 171–183 (2000).

88. Marquer, C. *et al.* Increasing membrane cholesterol of neurons in culture recapitulates Alzheimer's disease early phenotypes. *Mol. Neurodegener.* **9**, 60 (2014).

89. Lee, S.-I. *et al.* APOE4-carrying human astrocytes oversupply cholesterol to promote

neuronal lipid raft expansion and Aβ generation. *Stem cell reports* **16**, 2128–2137 (2021).

90. Tian, G., Kong, Q., Lai, L., Ray-Chaudhury, A. & Lin, C. G. Increased expression of cholesterol 24S-hydroxylase results in disruption of glial glutamate transporter EAAT2 association with lipid rafts: a potential role in Alzheimer's disease. *J. Neurochem.* **113**, 978–989 (2010).
91. Yang, X., Sun, G. Y., Eckert, G. P. & Lee, J. C.-M. Cellular membrane fluidity in amyloid precursor protein processing. *Mol. Neurobiol.* **50**, 119–129 (2014).
92. Christian, A. E., Haynes, M. P., Phillips, M. C. & Rothblat, G. H. Use of cyclodextrins for manipulating cellular cholesterol content. *J. Lipid Res.* **38**, 2264–2272 (1997).
93. Robichaud, S. & Ouimet, M. Quantifying Cellular Cholesterol Efflux BT - Lipid-Activated Nuclear Receptors: Methods and Protocols. in (eds. Gage, M. C. & Pineda-Torra, I.) 111–133 (Springer New York, 2019). doi:10.1007/978-1-4939-9130-3_9
94. BLIGH, E. G. & DYER, W. J. A rapid method of total lipid extraction and purification. *Can. J. Biochem. Physiol.* **37**, 911–917 (1959).
95. Elrick, H. *et al.* The production of 4,182 mouse lines identifies experimental and biological variables impacting Cas9-mediated mutant mouse line production. (2021). doi:10.1101/2021.10.06.463037
96. Gertsenstein, M. & Nutter, L. M. J. Engineering Point Mutant and Epitope-Tagged Alleles in Mice Using Cas9 RNA-Guided Nuclease. *Curr. Protoc. Mouse Biol.* **8**, 28–53 (2018).
97. Koscielny, G. *et al.* The International Mouse Phenotyping Consortium Web Portal, a unified point of access for knockout mice and related phenotyping data. *Nucleic Acids Res.* **42**, D802-9 (2014).
98. Forest, A. *et al.* Comprehensive and Reproducible Untargeted Lipidomic Workflow Using LC-QTOF Validated for Human Plasma Analysis. *J. Proteome Res.* **17**, 3657–3670 (2018).
99. Ruiz, M. *et al.* Lipidomics unveils lipid dyshomeostasis and low circulating plasmalogens as biomarkers in a monogenic mitochondrial disorder. *JCI insight* **4**, (2019).
100. Godzien, J. *et al.* Rapid and Reliable Identification of Phospholipids for Untargeted Metabolomics with LC-ESI-QTOF-MS/MS. *J. Proteome Res.* **14**, 3204–3216 (2015).
101. Robichaud, S. *et al.* Identification of novel lipid droplet factors that regulate lipophagy

and cholesterol efflux in macrophage foam cells. *Autophagy* 1–19 (2021). doi:10.1080/15548627.2021.1886839

102. Deutsch, E. W. *et al.* A guided tour of the Trans-Proteomic Pipeline. *Proteomics* **10**, 1150–1159 (2010).
103. Chambers, M. C. *et al.* A cross-platform toolkit for mass spectrometry and proteomics. *Nature biotechnology* **30**, 918–920 (2012).
104. Eng, J. K., Jahan, T. A. & Hoopmann, M. R. Comet: an open-source MS/MS sequence database search tool. *Proteomics* **13**, 22–24 (2013).
105. UniProt: the universal protein knowledgebase in 2021. *Nucleic Acids Res.* **49**, D480–D489 (2021).
106. Keller, A., Nesvizhskii, A. I., Kolker, E. & Aebersold, R. Empirical statistical model to estimate the accuracy of peptide identifications made by MS/MS and database search. *Anal. Chem.* **74**, 5383–5392 (2002).
107. Nesvizhskii, A. I., Keller, A., Kolker, E. & Aebersold, R. A statistical model for identifying proteins by tandem mass spectrometry. *Anal. Chem.* **75**, 4646–4658 (2003).
108. Shteynberg, D. *et al.* iProphet: multi-level integrative analysis of shotgun proteomic data improves peptide and protein identification rates and error estimates. *Mol. Cell. Proteomics* **10**, M111.007690 (2011).
109. Nadeau, R., Byvsheva, A. & Lavallée-Adam, M. PIGNON: a protein–protein interaction-guided functional enrichment analysis for quantitative proteomics. *BMC Bioinformatics* **22**, 302 (2021).
110. Supek, F., Bošnjak, M., Škunca, N. & Šmuc, T. REVIGO summarizes and visualizes long lists of gene ontology terms. *PLoS One* **6**, e21800 (2011).
111. Lein, E. S. *et al.* Genome-wide atlas of gene expression in the adult mouse brain. *Nature* **445**, 168–176 (2007).
112. Wang, Y.-H., Liu, C.-L., Chiu, W.-C., Twu, Y.-C. & Liao, Y.-J. HMGCS2 Mediates Ketone Production and Regulates the Proliferation and Metastasis of Hepatocellular Carcinoma. *Cancers (Basel).* **11**, (2019).
113. Caldas, H. & Herman, G. E. NSDHL, an enzyme involved in cholesterol biosynthesis,

traffics through the Golgi and accumulates on ER membranes and on the surface of lipid droplets. *Hum. Mol. Genet.* **12**, 2981–2991 (2003).

114. Ye, Z. *et al.* LRP6 protein regulates low density lipoprotein (LDL) receptor-mediated LDL uptake. *J. Biol. Chem.* **287**, 1335–1344 (2012).
115. Chang, T.-Y., Li, B.-L., Chang, C. C. Y. & Urano, Y. Acyl-coenzyme A:cholesterol acyltransferases. *Am. J. Physiol. Endocrinol. Metab.* **297**, E1-9 (2009).
116. Kontush, A., Lhomme, M. & Chapman, M. J. Unraveling the complexities of the HDL lipidome. *J. Lipid Res.* **54**, 2950–2963 (2013).
117. Camporesi, E. *et al.* Neuroligin-1 in brain and CSF of neurodegenerative disorders: investigation for synaptic biomarkers. *Acta Neuropathol. Commun.* **9**, 19 (2021).
118. Dufort-Gervais, J. *et al.* Neuroligin-1 is altered in the hippocampus of Alzheimer's disease patients and mouse models, and modulates the toxicity of amyloid-beta oligomers. *Sci. Rep.* **10**, 6956 (2020).
119. Sichler, M. E., Löw, M. J., Schleicher, E. M., Bayer, T. A. & Bouter, Y. Reduced Acoustic Startle Response and Prepulse Inhibition in the Tg4-42 Model of Alzheimer's Disease. *J. Alzheimer's Dis. Reports* **3**, 269–278 (2019).
120. Badhwar, A., Lerch, J. P., Hamel, E. & Sled, J. G. Impaired structural correlates of memory in Alzheimer's disease mice. *NeuroImage. Clin.* **3**, 290–300 (2013).
121. Ricci, G., Volpi, L., Pasquali, L., Petrozzi, L. & Siciliano, G. Astrocyte-neuron interactions in neurological disorders. *J. Biol. Phys.* **35**, 317–336 (2009).
122. Barber, C. N. & Raben, D. M. Lipid Metabolism Crosstalk in the Brain: Glia and Neurons. *Front. Cell. Neurosci.* **13**, 212 (2019).
123. Liu, L. *et al.* Glial lipid droplets and ROS induced by mitochondrial defects promote neurodegeneration. *Cell* **160**, 177–190 (2015).
124. Kim, J. *et al.* microRNA-33 Regulates ApoE Lipidation and Amyloid-β Metabolism in the Brain. *J. Neurosci. Off. J. Soc. Neurosci.* **35**, 14717–14726 (2015).
125. Wang, X. *et al.* Downregulation of miR-33 Has Protective Effect Against $A\beta_{25-35}$-Induced Injury in SH-SH-SY5Y Cells. *Med. Sci. Monit. Int. Med. J. Exp. Clin. Res.* **26**, e921026 (2020).

126. Meilandt, W. J. *et al.* Neprilysin overexpression inhibits plaque formation but fails to reduce pathogenic Abeta oligomers and associated cognitive deficits in human amyloid precursor protein transgenic mice. *J. Neurosci. Off. J. Soc. Neurosci.* **29**, 1977–1986 (2009).
127. Cui, M., Zhang, S., Liu, Y., Gang, X. & Wang, G. Grip Strength and the Risk of Cognitive Decline and Dementia: A Systematic Review and Meta-Analysis of Longitudinal Cohort Studies. *Frontiers in aging neuroscience* **13**, 625551 (2021).
128. Su, H., Sun, X., Li, F. & Guo, Q. Association between handgrip strength and cognition in a Chinese population with Alzheimer's disease and mild cognitive impairment. *BMC Geriatr.* **21**, 459 (2021).
129. Liu, J., Chang, L., Song, Y., Li, H. & Wu, Y. The Role of NMDA Receptors in Alzheimer's Disease. *Front. Neurosci.* **13**, 43 (2019).
130. Wang, R. & Reddy, P. H. Role of Glutamate and NMDA Receptors in Alzheimer's Disease. *J. Alzheimers. Dis.* **57**, 1041–1048 (2017).
131. Beal, E. Lipid biomarkers for early-stage Alzheimer disease. *Nat. Rev. Neurol.* **7**, 474 (2011).
132. Zhang, X., Liu, W., Zan, J., Wu, C. & Tan, W. Untargeted lipidomics reveals progression of early Alzheimer's disease in APP/PS1 transgenic mice. *Sci. Rep.* **10**, 14509 (2020).
133. Zhao, J., O'Connor, T. & Vassar, R. The contribution of activated astrocytes to Aβ production: implications for Alzheimer's disease pathogenesis. *J. Neuroinflammation* **8**, 150 (2011).
134. Frost, G. R. & Li, Y.-M. The role of astrocytes in amyloid production and Alzheimer's disease. *Open Biol.* **7**, (2017).
135. Crameri, A. *et al.* The role of seladin-1/DHCR24 in cholesterol biosynthesis, APP processing and Abeta generation in vivo. *EMBO J.* **25**, 432–443 (2006).
136. North, K. E., Martin, L. J., Dyer, T., Comuzzie, A. G. & Williams, J. T. HDL cholesterol in females in the Framingham Heart Study is linked to a region of chromosome 2q. *BMC Genet.* **4 Suppl 1**, S98 (2003).
137. Nissilä, E. *et al.* ORP10, a cholesterol binding protein associated with microtubules,

regulates apolipoprotein B-100 secretion. *Biochim. Biophys. Acta* **1821**, 1472–1484 (2012).

138. Teslovich, T. M. *et al.* Biological, clinical and population relevance of 95 loci for blood lipids. *Nature* **466**, 707–713 (2010).
139. Bouchard, L. *et al.* Association of OSBPL11 gene polymorphisms with cardiovascular disease risk factors in obesity. *Obesity (Silver Spring).* **17**, 1466–1472 (2009).
140. Koriyama, H. *et al.* Variation in OSBPL10 is associated with dyslipidemia. *Hypertens. Res.* **33**, 511–514 (2010).
141. Koriyama, H. *et al.* Identification of evidence suggestive of an association with peripheral arterial disease at the OSBPL10 locus by genome-wide investigation in the Japanese population. *J. Atheroscler. Thromb.* **17**, 1054–1062 (2010).
142. Perttilä, J. *et al.* OSBPL10, a novel candidate gene for high triglyceride trait in dyslipidemic Finnish subjects, regulates cellular lipid metabolism. *J. Mol. Med. (Berl).* **87**, 825–835 (2009).
143. Pedrini, S., Chatterjee, P., Hone, E. & Martins, R. N. High-density lipoprotein-related cholesterol metabolism in Alzheimer's disease. *J. Neurochem.* **159**, 343–377 (2021).
144. Balazs, Z. *et al.* Uptake and transport of high-density lipoprotein (HDL) and HDL-associated alpha-tocopherol by an in vitro blood-brain barrier model. *J. Neurochem.* **89**, 939–950 (2004).
145. Fung, K. Y. *et al.* SR-BI Mediated Transcytosis of HDL in Brain Microvascular Endothelial Cells Is Independent of Caveolin, Clathrin, and PDZK1. *Front. Physiol.* **8**, 841 (2017).
146. Sulliman, N. C. *et al.* HDL biodistribution and brain receptors in zebrafish, using HDLs as vectors for targeting endothelial cells and neural progenitors. *Sci. Rep.* **11**, 6439 (2021).

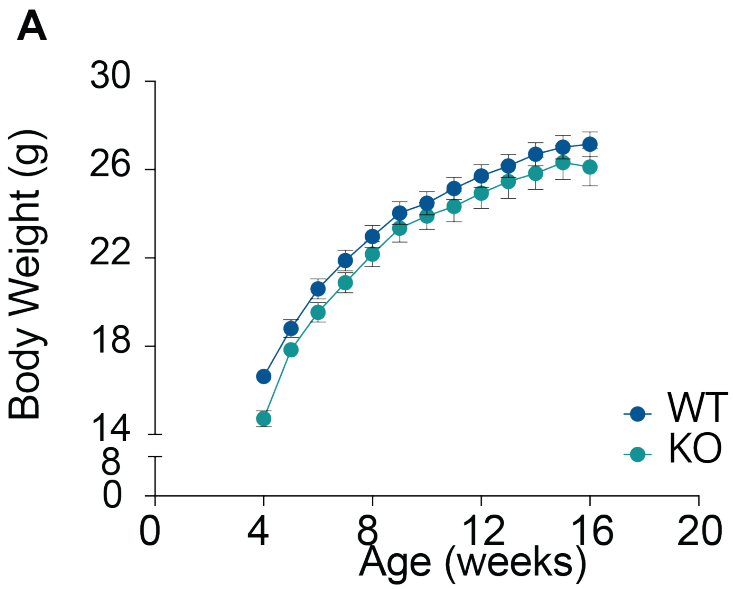

Supplemental Figure 1. WT and ORP6 deficient mice have no different in body weight (A) Body weight of Wild-type (blue) and *Osbpl6*$^{-/-}$ (green) mice (n=18-19 for WT and n=9 for *Osbpl6*$^{-/-}$ per sex, mean ± SEM) between 4 to 16 weeks.